A Riemannian quasi-Newton method for computing the Karcher mean of symmetric positive definite matrices

Xinru Yuan [*] Wen Huang [†§] P.-A. Absil [‡] K. A. Gallivan [*]

October 11, 2017

Abstract

This paper addresses the problem of computing the Karcher mean of a collection of symmetric positive definite matrices. We show in detail that the condition number of the Riemannian Hessian of the underlying optimization problem is never very ill conditioned in practice, which explains why the Riemannian steepest descent approach has been observed to perform well. We also show theoretically and empirically that this property is not shared by the Euclidean Hessian. Then we present a limited-memory Riemannian BFGS method to handle this computational task. We also provide methods to produce efficient numerical representations of geometric objects that are required for Riemannian optimization methods on the manifold of symmetric positive definite matrices. Through empirical results and a computational complexity analysis, we demonstrate the robust behavior of the limited-memory Riemannian BFGS method and the efficiency of our implementation when compared to state-of-the-art algorithms.

1 Introduction

Symmetric positive definite (SPD) matrices are fundamental objects in various domains. For example, a 3D diffusion tensor, i.e., a 3×3 SPD matrix, is commonly used to model the diffusion behavior of the media in diffusion tensor magnetic resonance imaging (DT-MRI) [9, 11, 32]. In addition, representing images and videos with SPD matrices has shown promise for segmentation and recognition in several studies, such as [4, 21, 28, 35, 36]. In these and similar applications, it is often of interest to average SPD matrices. Averaging is required, e.g., to aggregate several noisy measurements of the same object. It also appears as a subtask in interpolation methods [1], segmentation [5, 31], and clustering [23]. An efficient implementation of averaging method is crucial for applications where the mean computation must be done many times. For example, in K-means clustering, one needs to compute the means of each cluster in each iteration.

A natural way to average over a collection of SPD matrices, $\{A_1, \dots, A_K\}$, is to take their arithmetic mean, i.e., $G(A_1, \dots, A_K) = (A_1 + \cdots + A_K)/K$. However, this is not appropriate in applications where invariance under inversion is required, i.e., $G(A_1, \dots, A_K)^{-1} = G(A_1^{-1}, \dots, A_K^{-1})$. In addition, the arithmetic mean may cause a "swelling effect" that should be avoided in diffusion tensor imaging. Swelling is defined as an increase in the matrix determinant after averaging,

[*]Department of Mathematics, Florida State University, Tallahassee FL 32306-4510, USA
[†]Department of Computational and Applied Mathematics, Rice University, Houston, USA
[‡]Department of Mathematical Engineering, Université catholique de Louvain, Louvain-la-Neuve, Belgium.
[§]Corresponding author. E-mail: huwst08@gmail.com.

see [11] for example. An alternative is to generalize the definition of geometric mean from scalars to matrices, which yields $G(A_1, \dots, A_K) = (A_1 \dots A_K)^{1/K}$. However, this generalized geometric mean is not invariant under permutation since matrices are not commutative in general. Ando et al. [3] introduced a list of fundamental properties, referred to as the ALM list, that a matrix "geometric" mean should possess, such as invariance under permutation, monotonicity, congruence invariance, and invariance under inversion, to name a few. These properties are known to be important in numerous applications, e.g. [6, 27, 29]. However, they do not uniquely define a mean for $K \geq 3$. There can be many different definitions of means that satisfy all the properties. The Karcher mean proposed in [26] has been recognized as one of the most suitable means for SPD matrices in the sense that it satisfies all properties in the ALM list [6, 27].

1.1 Karcher mean

Let $\mathcal{S}_{++}^n$ be the manifold of $n \times n$ SPD matrices. Since $\mathcal{S}_{++}^n$ is an open submanifold of the vector space of $n \times n$ symmetric matrices, its tangent space at point X, denoted by $\mathrm{T}_X \mathcal{S}_{++}^n$, can be identified as the set of $n \times n$ symmetric matrices. The manifold $\mathcal{S}_{++}^n$ becomes a Riemannian manifold when endowed with the affine-invariant metric, see [31], given by

$$g_X(\xi_X, \eta_X) = \mathrm{trace}(\xi_X X^{-1} \eta_X X^{-1}). \tag{1.1}$$

The Karcher mean of $\{A_1, \dots, A_K\}$, also called the Riemannian center of mass, is the minimizer of the sum of squared distances

$$\mu = \underset{X \in \mathcal{S}_{++}^n}{\arg\min} F(X), \quad \text{with } F : \mathcal{S}_{++}^{\mathrm{n}} \to \mathbb{R},\ X \mapsto \frac{1}{2K} \sum_{i=1}^{K} \delta^2(X, A_i), \tag{1.2}$$

where $\delta(p, q) = \| \log(p^{-1/2} q p^{-1/2}) \|_{\mathrm{F}}$ is the geodesic distance associated with Riemannian metric (1.1). It is proved in [26] that function F has a unique minimizer. Hence a point $\mu \in \mathcal{S}_{++}^n$ is a Karcher mean if it is a stationary point of F, i.e., $\mathrm{grad}\, F(\mu) = 0$, where $\mathrm{grad}\, F$ denotes the Riemannian gradient of F under metric (1.1). However, a closed-form solution for problem (1.2) is unknown in general, and for this reason, the Karcher mean is usually computed by iterative methods.

1.2 Related work

Various methods have been used to compute the Karcher mean of SPD matrices. Most of them resort to the framework of Riemannian optimization (see, e.g., [2]), since problem (1.2) requires optimizing a function on a manifold. In particular, [25] presents a survey of several optimization algorithms, including Riemannian versions of steepest descent, conjugate gradient, BFGS, and trust-region Newton methods. The authors conclude that the first order methods, steepest descent and conjugate gradient, are the preferred choices for problem (1.2) in terms of time efficiency. The benefit of fast convergence of Newton's method and BFGS is nullified by their high computational costs per iteration, especially as the size of the matrices increases. It is also empirically observed in [25] that the Riemannian metric yields much faster convergence for their tested algorithms compared with the induced Euclidean metric, which is given by $g_X(\eta_X, \xi_X) = \mathrm{trace}(\xi_X \eta_X)$.

A Riemannian version of the Barzilai-Borwein method (RBB) has been considered in [22]. Several stepsize selection rules have been investigated for the Riemannian steepest descent (RSD)

method. A constant stepsize strategy is proposed in [34] and a convergence analysis is given. An adaptive stepsize selection rule based on the explicit expression of the Riemannian Hessian of the cost function F is studied in [33, Algorithm 2], which is actually the optimal stepsize for strongly convex function in Euclidean space, see [30, Theorem 2.1.14]. That is, the stepsize is chosen as $\alpha_k = 2/(M_k+L_k)$, where M_k and L_k are the lower and upper bounds on the eigenvalues of the Riemannian Hessian of F, respectively. A version of Newton method for the Karcher mean computation is also provided in [33]. A Richardson-like iteration is derived and evaluated empirically in [7], and is available in the Matrix Means Toolbox[1]. It is seen in Section 3.2 that the Richardson-like iteration is a steepest descent method with stepsize $\alpha_k = 1/L_k$.

1.3 Contributions

First, by providing lower and upper bounds on the condition number of the Riemannian and Euclidean Hessians of the cost function (1.2), we give a theoretical explanation for the above-mentioned behavior of the Riemannian and Euclidean steepest descent algorithms for SPD Karcher mean computation. Then we provide a detailed description of a limited-memory Riemannian BFGS (LRBFGS) method for this mean computation problem. Riemannian optimization methods such as LRBFGS involve manipulation of geometric objects on manifolds, such as tangent vectors, evaluation of a Riemannian metric, retraction, and vector transport. We present detailed methods to produce efficient numerical representations of those objects on the $\mathcal{S}_{++}^{\mathrm{n}}$ manifold. In fact, there are several alternatives to choose from for geometric objects on $\mathcal{S}_{++}^{\mathrm{n}}$. We offer theoretical and empirical suggestions on how to choose between those alternatives for LRBFGS based on computational complexity analysis and numerical experiments. Our numerical experiments indicate that as a result, and in spite of the favorable bound on the Riemannian Hessian that ensures Riemannian steepest descent to be an efficient method, the obtained LRBFGS method outperforms state-of-the-art methods on various instances of the problem. We also show that RBB is a special case of LRBFGS.

Another contribution of our work is to provide a C++ toolbox for the SPD Karcher mean computation, which includes LRBFGS, RBFGS, RBB, and RSD. The toolbox[2] relies on ROPTLIB, an object-oriented C++ library for optimization on Riemannian manifolds [19]. To the best of our knowledge, there is no other publicly available C++ toolbox for the SPD Karcher mean computation. Our previous work [38] provides a MATLAB implementation[3] for this problem. The Matrix Means Toolbox[1] developed by Bini et al. in [7] is also written in MATLAB. As an interpreted language, MATLAB's execution efficiency is lower than compiled languages, such as C++. In addition, the timing measurements in MATLAB can be skewed by MATLAB's overhead, especially for small-size problems. As a result, we resort to C++ for efficiency and reliable timing.

Finally, we test the performance of LRBFGS on problems of various sizes and conditioning, and compare with the state-of-the-art methods mentioned above. The size of a problem is characterized by the number of matrices as well as the dimension of each matrix, and the conditioning of the problem is characterized by the condition number of matrices. It is shown empirically that LRBFGS is appropriate for large-size problems or ill-conditioned problems. Especially when one has little knowledge of the conditioning of a problem, LRBFGS becomes the method of choice since it is robust to problem conditioning and parameter setting. The numerical results also illustrate the

[1] `http://bezout.dm.unipi.it/software/mmtoolbox/`
[2] `http://www.math.fsu.edu/~whuang2/papers/RMKMSPDM.htm`
[3] `http://www.math.fsu.edu/~whuang2/papers/ARLBACMGM.htm`

speedup of using C++ vs. MATLAB, especially for small-size problems. It is observed that the C++ implementation is faster than MATLAB by a factor of 100 or more with the factor gradually reducing as the size of the problem gets larger.

The paper is organized as follows. Section 2 studies the conditioning of the objective function (1.2) under the Riemannian metric and the Euclidean metric. Section 3 presents the implementation techniques for $\mathcal{S}_{++}^{\mathrm{n}}$ and computational complexity analysis. Detailed descriptions of the SPD Karcher mean computation methods considered (namely RL, RSD-QR, RBB, and LRBFGS) are given in Section 4. Numerical experiments are reported in Section 5. Conclusions are drawn in Section 6.

A preliminary version of some of the results presented in this paper can be found in the conference paper [38].

2 Conditioning of the objective function

The convergence speed of optimization methods depends on the conditioning of the Hessian of the cost function at the minimizer. Large values of condition number lead to slow convergence of optimization algorithms, especially for steepest descent methods. The choice of the metric has an important influence on the difficulty of an optimization problem via influencing the conditioning of the Hessian of the cost function. A good choice of metric may reduce the condition number of the Hessian.

Rentmeesters et al. [33, inequality (3.29)] gives bounds on the eigenvalues of the Riemannian Hessian of the squared distance function $f_A(X) = \frac{1}{2}\delta^2(X, A)$ given $A \in \mathcal{S}_{++}^{\mathrm{n}}$. On this basis, the bounds on the eigenvalues of the Riemannian Hessian of F can be obtained trivially. We summarize the results from [33] in Theorem 2.1 and, for completeness, we give the proof omitted by [33].

Theorem 2.1. *Let F be the objective function defined in problem (1.2) and $X \in \mathcal{S}_{++}^{\mathrm{n}}$. Then the eigenvalues of the Riemannian Hessian of F at X are bounded by*

$$1 \leq \frac{\operatorname{Hess} F(X)[\Delta X, \Delta X]}{\|\Delta X\|^2} \leq 1 + \frac{\log(\max_i \kappa_i)}{2}, \tag{2.1}$$

where κ_i denotes the condition number of matrix $X^{-1/2} A_i X^{-1/2}$ (or equivalently $L_x^{-1} A_i L_x^{-T}$ with $X = L_x L_x^T$ being the Cholesky decomposition of X).

Proof. The proof is a simple generalization from [33, inequality (3.29)], which gives bounds on the eigenvalues of the Riemannian Hessian of the function $f_A(X)$ as

$$1 \leq \frac{\operatorname{Hess} f_A(X)[\Delta X, \Delta X]}{\|\Delta X\|^2} \leq \frac{\log \kappa}{2} \coth(\frac{\log \kappa}{2}), \tag{2.2}$$

where κ is condition number of $X^{-1/2} A X^{-1/2}$. Notice that the objective function $F(X) = \frac{1}{K} \sum_{i=1}^{K} f_{A_i}(X)$. Thus, we have

$$1 \leq \frac{\operatorname{Hess} F(X)[\Delta X, \Delta X]}{\|\Delta X\|^2} \leq \frac{1}{K} \sum_{i=1}^{K} \frac{\log \kappa_i}{2} \coth(\frac{\log \kappa_i}{2}). \tag{2.3}$$

Since $x \coth(x)$ is strictly increasing and bounded by $1 + x$ on $[0, \infty]$, the right hand side of inequality (2.3) is thus bounded by $1 + \log(\max_i \kappa_i)/2$. $\square$

Theorem 2.1 implies that we cannot expect a very ill-conditioned Riemannian Hessian in practice. However, this is not the case when the Euclidean metric is used. In Theorem 2.2, we derive bounds on the condition number of the Euclidean Hessian of F at the minimizer. We need the following lemma before deriving the bounds.

Lemma 2.1. *Let $A \in \mathcal{S}_{++}^{\mathrm{n}}$ be a symmetric positive definite matrix with eigenvalues satisfying $0 < \lambda_1 \leq \lambda_2 \leq \cdots \leq \lambda_n$, and $\eta \in \mathbb{R}^{n\times n}$ be an $n \times n$ real symmetric matrix. Then, we have*

$$\max_{\eta=\eta^T} \frac{\operatorname{tr}(A\eta A\eta)}{\|\eta\|_{\mathrm{F}}^2} = \lambda_n^2, \ \textit{and} \ \min_{\eta=\eta^T} \frac{\operatorname{tr}(A\eta A\eta)}{\|\eta\|_{\mathrm{F}}^2} = \lambda_1^2. \tag{2.4}$$

Proof. Let $A = Q\Sigma Q^T$ be the eigenvalues decomposition of A, where $QQ^T = I$ and $\Sigma = \operatorname{diag}(\lambda_1, \ldots, \lambda_n)$. Then, we have

$$\frac{\operatorname{tr}(A\eta A\eta)}{\|\eta\|_{\mathrm{F}}^2} = \frac{\operatorname{tr}(Q\Sigma Q^T \eta^T Q\Sigma Q^T \eta)}{\|Q^T\eta Q\|_{\mathrm{F}}^2} = \frac{\operatorname{tr}(\Sigma\tilde{\eta}^T\Sigma\tilde{\eta})}{\|\tilde{\eta}\|_{\mathrm{F}}^2}. \tag{2.5}$$

Notice that we can rewrite the trace term on the right hand of equation (2.5) as

$$\operatorname{tr}(\Sigma\tilde{\eta}^T\Sigma\tilde{\eta}) = \operatorname{vec}(\tilde{\eta}\Sigma)^T \operatorname{vec}(\Sigma\eta) = \operatorname{vec}(\tilde{\eta})^T(I_n \otimes \Sigma)(\Sigma \otimes I_n)\operatorname{vec}(\tilde{\eta}) = \operatorname{vec}(\tilde{\eta})^T(\Sigma \otimes \Sigma)\operatorname{vec}(\tilde{\eta}). \tag{2.6}$$

On one hand, we have

$$\max_{\tilde{\eta}=\tilde{\eta}^T} \frac{\operatorname{tr}(\Sigma\tilde{\eta}^T\Sigma\tilde{\eta})}{\|\tilde{\eta}\|_{\mathrm{F}}^2} \leq \max_{\tilde{\eta}\in\mathbb{R}^{n\times n}} \frac{\operatorname{tr}(\Sigma\tilde{\eta}^T\Sigma\tilde{\eta})}{\|\tilde{\eta}\|_{\mathrm{F}}^2} = \max_{\tilde{\eta}\in\mathbb{R}^{n\times n}} \frac{\operatorname{vec}(\tilde{\eta})^T(\Sigma\otimes\Sigma)\operatorname{vec}(\tilde{\eta})}{\operatorname{vec}(\tilde{\eta})^T\operatorname{vec}(\tilde{\eta})} = \lambda_n^2. \tag{2.7}$$

The last equality comes from the fact that the eigenvalues of $\Sigma \otimes \Sigma$ are $\lambda_i\lambda_j$, $i = 1, \ldots, n$, $j = 1, \ldots, n$. On the other hand,

$$\max_{\tilde{\eta}=\tilde{\eta}^T} \frac{\operatorname{tr}(\Sigma\tilde{\eta}^T\Sigma\tilde{\eta})}{\|\tilde{\eta}\|_{\mathrm{F}}^2} \geq \frac{\operatorname{tr}(\Sigma\eta_0^T\Sigma\eta_0)}{\|\eta_0\|_{\mathrm{F}}^2} = \lambda_n^2, \tag{2.8}$$

where $\eta_0 = e_n e_n^T$ and $e_n = (0, \ldots, 0, 1)^T$. That is, η_0 is an $n \times n$ zero matrix except the (n, n) entry is 1. Combining inequalities (2.7) and (2.8), we obtain the first part of (2.4).

Similarly, we have

$$\min_{\tilde{\eta}=\tilde{\eta}^T} \frac{\operatorname{tr}(\Sigma\tilde{\eta}^T\Sigma\tilde{\eta})}{\|\tilde{\eta}\|_{\mathrm{F}}^2} \geq \min_{\tilde{\eta}\in\mathbb{R}^{n\times n}} \frac{\operatorname{tr}(\Sigma\tilde{\eta}^T\Sigma\tilde{\eta})}{\|\tilde{\eta}\|_{\mathrm{F}}^2} = \min_{\tilde{\eta}\in\mathbb{R}^{n\times n}} \frac{\operatorname{vec}(\tilde{\eta})^T(\Sigma\otimes\Sigma)\operatorname{vec}(\tilde{\eta})}{\operatorname{vec}(\tilde{\eta})^T\operatorname{vec}(\tilde{\eta})} = \lambda_1^2. \tag{2.9}$$

On the other hand, we let $\eta_0 = e_1 e_1^T$ and $e_1 = (1, 0, \ldots, 0)^T$. Then, we have

$$\min_{\tilde{\eta}=\tilde{\eta}^T} \frac{\operatorname{tr}(\Sigma\tilde{\eta}^T\Sigma\tilde{\eta})}{\|\tilde{\eta}\|_{\mathrm{F}}^2} \leq \frac{\operatorname{tr}(\Sigma\eta_0^T\Sigma\eta_0)}{\|\eta_0\|_{\mathrm{F}}^2} = \lambda_1^2. \tag{2.10}$$

Combining inequalities (2.9) and (2.10) immediately lead to the second part of (2.4). □

For notational simplicity, we use super script 'E' and 'R' to differentiate the Euclidean metric and the Riemannian metric.

Theorem 2.2. *Let $f : \mathcal{S}^{\mathrm{n}}_{++} \to \mathbb{R}$ be twice continuously differentiable and μ be a stationary point for f. Assume the largest and smallest eigenvalues of the Riemannian Hessian of f at μ are $\Lambda_{\max}$ and $\Lambda_{\min}$ respectively, i.e.,*

$$\Lambda_{\min} \leq \frac{\langle \operatorname{Hess}^{\mathrm{R}} f(\mu)[\eta], \eta\rangle^{\mathrm{R}}}{\langle \eta, \eta\rangle^{\mathrm{R}}} \leq \Lambda_{\max}. \tag{2.11}$$

Then the condition number of the Euclidean Hessian of f at μ, denoted by $\kappa(H^{\mathrm{E}})$, is bounded by

$$\frac{1}{\kappa(H^{\mathrm{R}})}\kappa^2(\mu) \leq \kappa(H^{\mathrm{E}}) \leq \kappa(H^{\mathrm{R}})\kappa^2(\mu), \tag{2.12}$$

where $\kappa(\mu)$ is the condition number of μ, and $\kappa(H^{\mathrm{R}}) = \Lambda_{\max}/\Lambda_{\min}$ is the condition number of the Riemannian Hessian of f at μ.

Proof. Recall that the condition number of the Euclidean Hessian of f at μ can be expressed as

$$\kappa(H^{\mathrm{E}}) = \max_{\eta=\eta^T} \frac{\langle \operatorname{Hess}^{\mathrm{E}} f(\mu)[\eta], \eta\rangle^{\mathrm{E}}}{\langle \eta, \eta\rangle^{\mathrm{E}}} / \min_{\eta=\eta^T} \frac{\langle \operatorname{Hess}^{\mathrm{E}} f(\mu)[\eta], \eta\rangle^{\mathrm{E}}}{\langle \eta, \eta\rangle^{\mathrm{E}}}, \tag{2.13}$$

and that of the Riemannian Hessian can be written in a similar way.

For any $X \in \mathcal{S}^{\mathrm{n}}_{++}$ and $\eta \in \mathrm{T}_X\, \mathcal{S}^{\mathrm{n}}_{++}$, the action of Hessian of f on η under the Riemannian metric is given by [25]

$$\operatorname{Hess}^{\mathrm{R}} f(X)[\eta] = \mathrm{D}(\operatorname{grad}^{\mathrm{R}} f)(X)[\eta] - \frac{1}{2}(\eta X^{-1} \operatorname{grad}^{\mathrm{R}} f(X) + \operatorname{grad}^{\mathrm{R}} f(X) X^{-1}\eta). \tag{2.14}$$

When $X = \mu$ is a stationary point of f, i.e., $\operatorname{grad}^{\mathrm{R}} f(\mu) = 0$, we have $\operatorname{Hess}^{\mathrm{R}} f(\mu)[\eta] = \mathrm{D}(\operatorname{grad}^{\mathrm{R}} f)(\mu)[\eta]$. As $\langle \operatorname{grad}^{\mathrm{E}} f(X), \eta\rangle^{\mathrm{E}} = \mathrm{D}\, f(X)[\eta] = \langle \operatorname{grad}^{\mathrm{R}} f(X), \eta\rangle^{\mathrm{R}}$, we have

$$\operatorname{grad}^{\mathrm{R}} f(X) = X \operatorname{grad}^{\mathrm{E}} f(X) X. \tag{2.15}$$

Therefore, equation (2.14) yields

$$\begin{aligned} \operatorname{Hess}^{\mathrm{R}} f(\mu)[\eta] &= \eta \operatorname{grad}^{\mathrm{E}} f(\mu)\mu + \mu(\mathrm{D}(\operatorname{grad}^{\mathrm{E}} f)(\mu)[\eta])\mu + \mu \operatorname{grad}^{\mathrm{E}} f(\mu)\eta & (2.16)\\ &= \mu(\mathrm{D}(\operatorname{grad}^{\mathrm{E}} f)(\mu)[\eta])\mu = \mu(\operatorname{Hess}^{\mathrm{E}} f(\mu)[\eta])\mu. & (2.17) \end{aligned}$$

This gives us

$$\langle \operatorname{Hess}^{\mathrm{R}} f(\mu)[\eta], \eta\rangle^{\mathrm{R}} = \operatorname{tr}(\mu^{-1} \operatorname{Hess}^{\mathrm{R}} f(\mu)[\eta]\mu^{-1}\eta) = \operatorname{tr}(\operatorname{Hess}^{\mathrm{E}} f(\mu)[\eta]\eta) = \langle \operatorname{Hess}^{\mathrm{E}} f(\mu)[\eta], \eta\rangle^{\mathrm{E}}. \tag{2.18}$$

It follows that

$$\frac{\langle \operatorname{Hess}^{\mathrm{E}} f(\mu)[\eta], \eta\rangle^{\mathrm{E}}}{\langle \eta, \eta\rangle^{\mathrm{E}}} = \frac{\langle \operatorname{Hess}^{\mathrm{R}} f(\mu)[\eta], \eta\rangle^{\mathrm{R}}}{\langle \eta, \eta\rangle^{\mathrm{R}}} \cdot \frac{\langle \eta, \eta\rangle^{\mathrm{R}}}{\langle \eta, \eta\rangle^{\mathrm{E}}}. \tag{2.19}$$

By assumption, we have

$$\Lambda_{\min} \leq \frac{\langle \operatorname{Hess}^{\mathrm{R}} f(\mu)[\eta], \eta\rangle^{\mathrm{R}}}{\langle \eta, \eta\rangle^{\mathrm{R}}} \leq \Lambda_{\max}. \tag{2.20}$$

Assume that the eigenvalues of μ are $0 < \lambda_1 \leq \cdots \leq \lambda_n$, and then the eigenvalues of μ^{-1} are $0 < 1/\lambda_n \leq \cdots \leq 1/\lambda_1$. From Lemma 2.1, we have

$$\max_{\eta=\eta^T} \frac{\langle \eta, \eta \rangle^{\mathrm{R}}}{\langle \eta, \eta \rangle^{\mathrm{E}}} = \frac{1}{\lambda_1^2} \text{ and } \min_{\eta=\eta^T} \frac{\langle \eta, \eta \rangle^{\mathrm{R}}}{\langle \eta, \eta \rangle^{\mathrm{E}}} = \frac{1}{\lambda_n^2}. \tag{2.21}$$

Multiplying inequality (2.20) and equation (2.21) gives

$$\frac{\Lambda_{\min}}{\lambda_1^2} \leq \max_{\eta=\eta^T} \frac{\langle \mathrm{Hess}^{\mathrm{E}} f(\mu)[\eta], \eta \rangle^{\mathrm{E}}}{\langle \eta, \eta \rangle^{\mathrm{E}}} \leq \frac{\Lambda_{\max}}{\lambda_1^2}, \tag{2.22}$$

and

$$\frac{\Lambda_{\min}}{\lambda_n^2} \leq \min_{\eta=\eta^T} \frac{\langle \mathrm{Hess}^{\mathrm{E}} f(\mu)[\eta], \eta \rangle^{\mathrm{E}}}{\langle \eta, \eta \rangle^{\mathrm{E}}} \leq \frac{\Lambda_{\max}}{\lambda_n^2}. \tag{2.23}$$

Dividing inequality (2.22) by (2.23) gives us the lower and upper bounds on the condition number of the Euclidean Hessian of f at stationary point μ:

$$\frac{\Lambda_{\min}}{\Lambda_{\max}} \frac{\lambda_n^2}{\lambda_1^2} \leq \kappa(H^{\mathrm{E}}) \leq \frac{\Lambda_{\max}}{\Lambda_{\min}} \frac{\lambda_n^2}{\lambda_1^2}. \tag{2.24}$$

That is,

$$\frac{1}{\kappa(H^{\mathrm{R}})} \kappa^2(\mu) \leq \kappa(H^{\mathrm{E}}) \leq \kappa(H^{\mathrm{R}}) \kappa^2(\mu). \tag{2.25}$$

□

Remark 2.1. *Notice that equality* (2.18) *can be simply obtained by the fact that* $\langle \mathrm{Hess}\, F(\mu)[\eta], \eta \rangle$ *is independent of the metric when* μ *is a critical point of* F*. The proof can be found in [2, Section 5.5].*

For the cost function F in (1.2), it is seen from Theorem 2.2 that the condition number of the Euclidean Hessian at the minimizer (stationary point) is bounded below by the square of the condition number of the minimizer scaled by the reciprocal of the condition number of the Riemannian Hessian of F. Hence when the minimizer is ill-conditioned, the Euclidean Hessian of F at the minimizer is ill-conditioned as well, which will slow down the optimization methods. Our numerical experiments in Section in 5.3 demonstrate this expectation.

3 Implementation for the $\mathcal{S}_{++}^{\mathrm{n}}$ manifold

This section is devoted to the implementation details of the required objects for Riemannian optimization methods on the SPD Karcher mean computation problem. Manifold-related objects include tangent vectors, the Riemannian metric, isometric vector transport, and retraction. Problem-related objects include the cost function and Riemannian gradient evaluations. As an extension of our previous work [38], we also provide a floating point operation (flop) count[4], for most operations.

[4] see [14, Section 1.2.4]

3.1 Representations of a tangent vector and the Riemannian metric

The $\mathcal{S}_{++}^n$ manifold can be viewed as a submanifold of $\mathbb{R}^{n\times n}$, and its tangent space at X is the set of symmetric matrices, i.e., $\mathrm{T}_X\,\mathcal{S}_{++}^n = \{S \in \mathbb{R}^{n\times n} | S = S^T\}$. The dimension of $\mathcal{S}_{++}^{\mathrm{n}}$ is $d = n(n+1)/2$. Thus, a tangent vector η_X in $\mathrm{T}_X\,\mathcal{S}_{++}^n$ can be represented either by an n^2-dimensional vector in Euclidean space $\mathcal{E}$, or a d-dimensional vector of coordinates in a given basis B_X of $\mathrm{T}_X\,\mathcal{S}_{++}^n$. The n^2-dimensional representation is called the extrinsic approach, and the d-dimensional one is called the intrinsic approach. For simplicity, we use w to denote the dimension of the embedding space, i.e., $w = n^2$.

The computational benefits of using intrinsic representation are addressed in [16, 17]: (i) Working in d-dimension reduces the computational complexity of linear operations on the tangent space. (ii) There exists an isometric vector transport, called vector transport by parallelization, whose intrinsic implementation is simply the identity. (iii) The Riemannian metric can be reduced to the Euclidean metric. However, the intrinsic representation requires a basis of tangent space, and in order to obtain the computational benefits mentioned above, it must be orthonormal. Hence, if a manifold admits a smooth field of orthonormal tangent space bases with acceptable computational complexity, the intrinsic representation often leads to a very efficient implementation. This property holds for $\mathcal{S}_{++}^n$ as shown next.

The orthonormal basis B_X of $\mathrm{T}_X\,\mathcal{S}_{++}^n$ that we select is given by

$$\{Le_ie_i^TL^T : i = 1, \ldots, n\} \bigcup \{\frac{1}{\sqrt{2}} L(e_ie_j^T + e_je_i^T)L^T,\ i < j,\ i = 1, \ldots, n,\ j = 1, \ldots, n\}, \tag{3.1}$$

where $X = LL^T$ denotes the Cholesky decomposition, and $\{e_1, \ldots, e_n\}$ is the standard basis of n-dimensional Euclidean space. Another choice is to use the matrix square root $X^{1/2}$ instead of Cholesky decomposition of X, which however costs more [15]. It is easy to verify the orthonormality of B_X under the Riemannian metric (1.1), i.e., $B_X^\flat B_X = I_{d\times d}$ for all $X \in \mathcal{S}_{++}^{\mathrm{n}}$. (The notation $a^\flat$ denotes the function $a^\flat : \mathrm{T}_X\,\mathcal{M} \to \mathbb{R} : v \mapsto g_X(a, v)$, where g stands for the Riemannian metric (1.1).) We assume throughout the paper that B_X stands for our selected orthonormal basis of $\mathrm{T}_X\,\mathcal{S}_{++}^n$ defined in (3.1).

Let η_X be a tangent vector in $\mathrm{T}_X\,\mathcal{S}_{++}^{\mathrm{n}}$ and v_X be its intrinsic representation. We define function $E2D_X : \eta_X \mapsto v_X = B_X^\flat \eta_X$ that maps the extrinsic representation to the intrinsic representation. Using the orthonormal basis defined in (3.1), the intrinsic representation of η_X is obtained by taking the diagonal elements of $L^{-1}\eta_X L^{-T}$, and its upper triangular elements row-wise and multiplied by $\sqrt{2}$. A detailed description of function $E2D$ is given in Algorithm 1. The number of flops for each step is given on the right of the algorithm.

Since B_X forms an orthonormal basis of $\mathrm{T}_X\,\mathcal{S}_{++}^{\mathrm{n}}$, the Riemannian metric (1.1) reduces to the Euclidean metric under the intrinsic representation, i.e.,

$$\tilde{g}_X(v_X, u_X) := g_X(\eta_X, \xi_X) = g_X(B_Xv_X, B_Xu_X) = v_X^T u_X, \tag{3.2}$$

where $\eta_X = B_Xv_X$, $\xi_X = B_Xu_X \in \mathrm{T}_X\,\mathcal{S}_{++}^{\mathrm{n}}$. The evaluation of (3.2) requires $2d$ flops, which is cheaper than the evaluation of (1.1).

For the intrinsic approach, retractions (see Section 3.2) require mapping the intrinsic representation back to the extrinsic representation, which may need extra work. Let function $D2E_X : v_X \mapsto \eta_X = B_Xv_X$ denote this mapping. In practice, the function $D2E_X$ using basis (3.1) is described in Algorithm 2.

Algorithm 1 Compute $E2D_X(\eta_X)$

Input: $X = LL^T \in \mathcal{S}_{++}^{\mathrm{n}}$, $\eta_x \in \mathrm{T}_X\, \mathcal{S}_{++}^{\mathrm{n}}$.

1: Compute $Y = L^{-1}\eta_X$ by solving linear system $LY = \eta_X$; ▷ # n^3

2: $Y \leftarrow Y^T$ (i.e., $Y = \eta_X L^{-T}$) ;

3: Compute $Z = L^{-1}\eta_X L^{-T}$ by solving linear system $LZ = Y$; ▷ # n^3

4: return $v_X = (z_{11}, \dots, z_{nn}, \sqrt{2}z_{12}, \dots, \sqrt{2}z_{1n}, \sqrt{2}z_{23}, \dots, \sqrt{2}z_{2n}, \dots, \sqrt{2}z_{(n-1)n})^T$; ▷ # d

Algorithm 2 Compute $D2E_X(v_X)$

Input: $X = LL^T \in \mathcal{S}_{++}^{\mathrm{n}}$, $v_x \in \mathbb{R}^{n(n+1)/2}$.

1: $\eta_{ii} = v_X(i)$ for $i = 1, \dots, n$; ▷ # n

2: $k = n + 1$;

3: **for** $i = 1, \dots, n$ **do** ▷ # $n^2 - n(n+1)/2$

4: **for** $j = i + 1, \dots, n$ **do**

5: $\eta_{ij} = v_X(k)$ and $\eta_{ji} = v_X(k)$;

6: $k = k + 1$;

7: **end for**

8: **end for**

9: return $L\eta L^T$; ▷ # $2n^3$

3.2 Retraction and vector transport

The concepts of retraction and vector transport can be found in [2]. A retraction is a smooth mapping R from the tangent bundle $\mathrm{T}\,\mathcal{M}$ onto $\mathcal{M}$ such that (i) $R(0_x) = x$ for all $x \in \mathcal{M}$ (where 0_x denotes the origin of $\mathrm{T}_x\,\mathcal{M}$) and (ii) $\frac{d}{dt}R(t\xi_x)|_{t=0} = \xi_x$ for all $\xi_x \in \mathrm{T}_x\,\mathcal{M}$. A vector transport $\mathcal{T} : \mathrm{T}\,\mathcal{M} \oplus \mathrm{T}\,\mathcal{M} \to \mathrm{T}\,\mathcal{M}$, $(\eta_x, \xi_x) \mapsto \mathcal{T}_{\eta_x}\xi_x$ with associated retraction R is a smooth mapping such that, for all (x, η_x) in the domain of R and ξ_x, $\zeta_x \in \mathrm{T}_x\,\mathcal{M}$, it holds that (i) $\mathcal{T}_{\eta_x}\xi_x \in \mathrm{T}_{R(\eta_x)}\,\mathcal{M}$, (ii) $\mathcal{T}_{0_x}\xi_x = \xi_x$, (iii) $\mathcal{T}_{\eta_x}$ is a linear map. Some methods, such as RBFGS in [20, Algorithm 1] and LRBFGS, require the vector transport to be isometric, i.e., $g_{R(\eta_x)}(\mathcal{T}_{S_{\eta_x}}\xi_x, \mathcal{T}_{S_{\eta_x}}\zeta_x) = g_x(\xi_x, \zeta_x)$. Throughout the paper, we use the notation $\mathcal{T}_S$ for isometric vector transport.

The choice of retraction and vector transport is a key step in the design of efficient Riemannian optimization algorithms. The exponential mapping is a natural choice for retraction. When $\mathcal{S}_{++}^n$ is endowed with the Riemannian metric (1.1), the exponential mapping is given by, see [12],

$$\mathrm{Exp}_X(\eta_X) = X^{1/2}\exp(X^{-1/2}\eta_X X^{-1/2})X^{1/2}, \tag{3.3}$$

for all $X \in \mathcal{S}_{++}^n$ and $\eta_X \in \mathrm{T}_X\,\mathcal{S}_{++}^n$. In practice, the exponential mapping (3.3) is expensive to compute. The exponential of matrix M is computed as $\exp(M) = U\exp(\Sigma)U^T$, with $M = U\Sigma U^T$ being the eigenvalue decomposition. Obtaining Σ and U by Golub-Reinsch algorithm requires $12n^3$ flops, see [14, Figure 8.6.1]. Hence the evaluation of $\exp(M)$ requires $16n^3$ flops in total. More importantly, when computing the matrix exponential $\exp(M)$, eigenvalues of large magnitude can lead to numerical difficulties. Jeuris et al. [25] proposed a retraction

$$R_X(\eta_X) = X + \eta_X + \frac{1}{2}\eta_X X^{-1}\eta_X, \tag{3.4}$$

which is a second order approximation to the exponential mapping (3.3). Retraction (3.4) is cheaper

to compute and requires $3n^3 + o(n^3)$ flops, and tends to avoid numerical overflow. An important property of retraction (3.4) is stated in Proposition 3.1.

Proposition 3.1. *Retraction $R_X(\eta)$ defined in* (3.4) *remains symmetric positive definite for all $X \in \mathcal{S}_{++}^n$ and $\eta \in \mathrm{T}_X\, \mathcal{S}_{++}^{\mathrm{n}}$.*

Proof. For all $v \neq 0$, $X \in \mathcal{S}_{++}^{\mathrm{n}}$, and $\eta \in \mathrm{T}_X\, \mathcal{S}_{++}^{\mathrm{n}}$, we have

$$\begin{aligned} v^T R_X(\eta) v &= \frac{1}{2} v^T (X + 2\eta + \eta X^{-1} \eta) v + \frac{1}{2} v^T X v \\ &= \frac{1}{2} v^T (X^{1/2} + \eta X^{-1/2})(X^{1/2} + \eta X^{-1/2})^T v + \frac{1}{2} v^T X v > 0. \end{aligned} \tag{3.5}$$

□

Another retraction that can be computed efficiently is the first order approximation to (3.3), i.e.,

$$R_X(\eta_X) = X + \eta_X. \tag{3.6}$$

In fact, retraction (3.6) is the exponential mapping when $\mathcal{S}_{++}^{\mathrm{n}}$ is endowed with the Euclidean metric. However, the result of retraction (3.6) is not guaranteed to be positive definite. Therefore one must be careful when using this Euclidean retraction. One remedy is to reduce the stepsize when necessary. The Richardson-like iteration in [7] is a steepest descent method using Euclidean retraction (3.6).

Parallel translation is a particular instance of vector transport. The parallel translation on $\mathcal{S}_{++}^n$ is given by, see [12],

$$\mathcal{T}_{p_{\xi_X}}(\eta_X) = X^{1/2} \exp\left(\frac{X^{-1/2} \xi_X X^{-1/2}}{2}\right) X^{-1/2} \eta_X X^{-1/2} \exp\left(\frac{X^{-1/2} \xi_X X^{-1/2}}{2}\right) X^{1/2}. \tag{3.7}$$

The computation of parallel translation involves the matrix exponential, which is computationally expensive. Note, however, that if parallel translation is used together with the exponential mapping (3.3), the most expensive exponential computation can be shared by rewriting (3.7) and (3.3) as shown in Algorithm 4. Even so, the matrix exponential computation is still required. We thus resort to another vector transport.

Recently, Huang et al. [16, Section 2.3.1] proposed a novel way to construct an isometric vector transport, called vector transport by parallelization. It is defined by

$$\mathcal{T}_S = B_Y B_X^\flat, \tag{3.8}$$

where B_X and B_Y are orthonormal bases of $\mathrm{T}_X\, \mathcal{S}_{++}^{\mathrm{n}}$ and $\mathrm{T}_Y\, \mathcal{S}_{++}^{\mathrm{n}}$ defined in (3.1) respectively. Let $v_X = B_X^\flat \eta_X$ be the intrinsic representation of η_X. Then, the intrinsic approach of (3.8), denoted by $\mathcal{T}_S^d$, is given by

$$\mathcal{T}_S^d v_X = B_Y^\flat \mathcal{T}_S \eta_X = B_Y^\flat B_Y B_X^\flat B_X v_X = v_X \tag{3.9}$$

That is, the intrinsic representation of vector transport by parallelization is simply the identity, which is the cheapest vector transport one can expect.

Another possible choice for the vector transport is the identity mapping: $\mathcal{T}_{id_{\xi_X}}(\eta_X) = \eta_X$. However, vector transport $\mathcal{T}_{id}$ is not applicable to the LRBFGS in [20, Algorithm 2] since it is not isometric under Riemannian metric (1.1).

Given a retraction, Huang et al. [20, Section 2] provides a method to construct an isometric vector transport such that the pair satisfies the locking condition[5], denoted by $\mathcal{T}_L$, which is given by

$$\mathcal{T}_{L_{\xi_X}} \eta_X = B_Y (I - \frac{2 v_2 v_2^T}{v_2^T v_2})(I - \frac{2 v_1 v_1^T}{v_1^T v_1}) B_1^\flat \eta_X, \tag{3.10}$$

where $v_1 = B_X^\flat \xi_X - z$, $v_2 = z - \beta B_Y^\flat \mathcal{T}_{R_{\xi_X}} \xi_X$, $\beta = \|\xi_X\| / \|\mathcal{T}_{R_{\xi_X}} \xi_X\|$, and $\mathcal{T}_R$ denotes the differentiated retraction. z can be any tangent vector satisfying $\|z\| = \|B_1^\flat \xi_X\| = \|\beta B_2^\flat \mathcal{T}_{R_{\xi_X}} \xi_X\|$. $z = -B_1^\flat \xi_X$ and $z = -\beta B_2^\flat \xi_X$ are natural choices. The intrinsic representation of (3.10) is given by

$$\begin{aligned} \mathcal{T}_L^d v_X &= B_Y^\flat B_Y (I - \frac{2 v_2 v_2^T}{v_2^T v_2})(I - \frac{2 v_1 v_1^T}{v_1^T v_1}) B_1^\flat \eta_X \quad (3.11)\\ &= (I - \frac{2 v_2 v_2^T}{v_2^T v_2})(I - \frac{2 v_1 v_1^T}{v_1^T v_1}) v_X. \quad (3.12) \end{aligned}$$

The evaluation of the intrinsic vector transport (3.12) requires $12d$ flops, i.e., $6n^2$.

3.3 Riemannian gradient of the sum of squared distances function

The cost function (1.2) can be rewritten as

$$f(X) = \frac{1}{2K} \sum_{i=1}^{K} \| \log(A_i^{-1/2} X A_i^{-1/2}) \|_F^2 = \frac{1}{2K} \sum_{i=1}^{K} \| \log(L_{A_i}^{-1} X L_{A_i}^{-T}) \|_F^2 \tag{3.13}$$

where $A_i = L_{A_i} L_{A_i}^T$. We use Cholesky decomposition rather than the matrix square root due to computational efficiency. The matrix logarithm is computed in a similar way as the exponential, i.e., $\log(M) = U \log(\Sigma) U^T$ with $M = U \Sigma U^T$ being the eigenvalue decomposition. So the number of flops required by the evaluation of (3.13) is $18Kn^3$.

The Riemannian gradient of the cost function F in (1.2) is given by, see [26],

$$\operatorname{grad} F(X) = -\frac{1}{K} \sum_{i=1}^{K} \operatorname{Exp}_X^{-1}(A_i), \tag{3.14}$$

where $\operatorname{Exp}_X^{-1}(Y)$ is the log-mapping, i.e., the inverse exponential mapping. On $\mathcal{S}_{++}^n$, the log-mapping is computed as

$$\operatorname{Exp}_X^{-1}(Y) = X^{1/2} \log(X^{-1/2} Y X^{-1/2}) X^{1/2} = \log(Y X^{-1}) X. \tag{3.15}$$

Note that the computational complexity of the Riemannian gradient is less than that conveyed in formula (3.15) since the most expensive logarithm computation is already available from the evaluation of the cost function at X. Specifically, each term in (3.14) is computed as $-\operatorname{Exp}_X^{-1}(A_i) = -\log(A_i X^{-1}) X = \log(X A_i^{-1}) X = L_{A_i} \log(L_{A_i}^{-1} X L_{A_i}^{-T}) L_{A_i}^{-1} X$, and the term $\log(L_{A_i}^{-1} X L_{A_i}^{-T})$ is available from the evaluation of the cost function $F(X)$ in (3.13). Hence the computation of gradient requires $5Kn^3$ flops if $\log(L_{A_i}^{-1} X L_{A_i}^{-T})$ is given.

[5] see [20, Section 2 Equation (2.8)] for the definition of the locking condition

4 Description of the SPD Karcher mean computation methods

In this section, we present the algorithms for SPD Karcher mean computation, including a limited-memory Riemannian BFGS (LRBFGS) [20], Riemannian Barzilai-Borwein (RBB) [22], Riemannian steepest descent with stepsize selection rule proposed by Q. Rentmeesters (RSD-QR) [33], and a Richardson-like iteration (RL) [7]. All of the algorithms are retraction-based methods, namely, an iterate x_k on a manifold $\mathcal{M}$ is updated by

$$x_{k+1} = R_{x_k}(\alpha_k \eta_k), \tag{4.1}$$

where R is a retraction on $\mathcal{M}$, $\eta_k \in \mathrm{T}_{x_k}\mathcal{M}$ is the search direction and $\alpha_k \in \mathbb{R}$ denotes the stepsize.

For the steepest descent method, the search direction in (4.1) is taken as the negative gradient, i.e., $\eta_k = -\operatorname{grad} f(x_k)$. RSD-QR for the SPD Karcher mean computation is summarized in Algorithm 3 based on [33, Algorithm 2]. The differences between RSD-QR and RL are the choice of stepsize strategy in Step 11 and the retraction in Step 13 of Algorithm 3. For RL, the stepsize is taken as $\alpha_{RL} = 1/\Delta$, where Δ is the upper bound on the eigenvalues of the Hessian of the cost function as computed in Step 10, and the Euclidean retraction (3.6) is used. The number of flops required per iteration is $22Kn^3 + o(Kn^3)$. For RSD-QR, the chosen stepsize is $\alpha_{QR} = 2/(U + \Delta)$, where $U = 1$ is the lower bound on the eigenvalues of the Hessian of the cost function. It is easy to verify that $1/\Delta \leq 2/(1+\Delta)$, with equality when $\Delta = 1$. Since the eigenvalues of the Hessian of the cost function are bounded by U and Δ, then $\Delta = 1$ implies that all the eigenvalues of the Hessian are exactly 1. So $\alpha_{RL} = \alpha_{QR}$ if and only if the Hessian of the cost function is the identity matrix, and we have $\alpha_{RL} < \alpha_{QR}$ in general. The exponential mapping (3.3) is used by RSD-QR in [33]. In practice, we use retraction (3.4), since the exponential mapping contains matrix exponential evaluation, and it turns out to be a problem if the eigenvalues of matrices in some intermediate iterations become too large, resulting in numerical overflow. Then each iteration in RSD-QR needs $22Kn^3 + 4/3n^3 + o(Kn^3)$ flops. Even though RSD-QR is slightly more expensive per iteration than RL, it will be seen in our experiments to require fewer iterations to achieve a desired tolerance, to perform very well on small-size problems in terms of time efficiency, and to consistently outperform RL in various situations.

RBB also belongs to the class of steepest descent methods, combined with a stepsize that makes implicit use of second order information of the cost function, see [10, 22] for details. The two most frequently used versions of the BB stepsize are

$$\alpha_{k+1}^{\mathrm{BB1}} = \frac{g(s_k, s_k)}{g(s_k, y_k)}, \tag{4.2}$$

$$\alpha_{k+1}^{\mathrm{BB2}} = \frac{g(s_k, y_k)}{g(y_k, y_k)}, \tag{4.3}$$

where $s_k = \mathcal{T}_{\alpha_k\eta_k}(\alpha_k\eta_k)$, $y_k = \operatorname{grad} f(x_{k+1}) - \mathcal{T}_{\alpha_k\eta_k}(\operatorname{grad} f(x_k))$, and $g(s_k, y_k) > 0$. An adaptive BB stepsize selection rule given in [13], denoted by $\mathrm{ABB_{min}}$, is defined as

$$\alpha_{k+1}^{\mathrm{ABB_{min}}} = \begin{cases} \min\{\alpha_j^{\mathrm{BB2}} : j = \max(1, k - m_a), \ldots, k\}, & \text{if } \dfrac{\alpha_{k+1}^{\mathrm{BB2}}}{\alpha_{k+1}^{\mathrm{BB1}}} < \tau \\ \alpha_{k+1}^{\mathrm{BB1}}, & \text{otherwise} \end{cases} \tag{4.4}$$

where m_a is a nonnegative integer and $\tau \in (0, 1)$.

Algorithm 3 RSD for the SPD Karcher mean computation

Input: $A_i = L_{A_i} L_{A_i}^T$; tolerance for stopping criteria ϵ; initial iterate $x_0 \in \mathcal{S}_{++}^{\mathrm{n}}$;

1: $k = 0$;
2: **while** $\|\operatorname{grad} f(x_k)\| > \epsilon$ **do**
3: **for** $i = 1, \ldots, K$ **do**
4: Compute $M_i = L_{A_i}^{-1} x_k L_{A_i}^{-T}$; ▷ # $2n^3$
5: Compute $M_i = U \Sigma U^{-1}$ and set $\lambda = \operatorname{diag}(\Sigma)$; ▷ # $12n^3$
6: Compute the condition number $c_i = \max(\lambda)/\min(\lambda)$; ▷ # 1
7: Compute $K_i = U \log(\Sigma) U^{-1}$; ▷ # $4n^3$
8: Compute $G_i = L_{A_i} K_i L_{A_i}^{-1} x_k$; ▷ # $4n^3$
9: **end for**
10: Compute the upper bound on the eigenvalues of the Hessian of the cost function: $\Delta = \frac{1}{K} \sum_{j=1}^{K} \frac{\log c_j}{2} \coth(\frac{\log c_j}{2})$; ▷ # $5K$
11: Compute stepsize $\alpha_k = \alpha(\Delta)$;
12: Compute $\operatorname{grad} f(x_k) = \frac{1}{K} \sum_{i=1}^{K} G_i$; ▷ # $(K+1)n^2$
13: Compute $x_{k+1} = R_{x_k}(-\alpha_k \operatorname{grad} f(x_k))$;
14: $k = k + 1$;
15: **end while**

In [22], RBB based on (4.2) has been applied to the SPD Karcher mean computation. We summarize that implementation in Algorithm 4, which uses an extrinsic representation of a tangent vector, exponential mapping (3.3) and parallel translation (3.7). Algorithm 5 states our implementation of RBB using the intrinsic representation approach, retraction (3.4) and vector transport by parallelization (3.9). We present the number of flops for each step on the right-hand side of the algorithms, except problem-related operations, i.e., function, gradient evaluations and line search procedure. Note that Step 7 and Step 11 in Algorithm 4 share the common term $\exp(\alpha_k x_k^{-1} \eta_k)$, which dominates the computational time and is only computed once. Having $w = n^2$ and $d = n(n+1)/2$, the number of flops per iteration for Algorithm 4 and Algorithm 5 are $103n^3/3 + o(n^3)$ and $22n^3/3 + o(n^3)$ respectively. The number of flops required by Algorithm 5 is smaller than that of Algorithm 4, and the computational efficiency mainly comes from the choice of retraction and the fact that the Riemannian metric reduces to the Euclidean metric when the intrinsic representation of a tangent vector is used.

Our previous work [38] tailors the LRBFGS in [20, Algorithm 2] to the SPD Karcher mean computation problem. The limited-memory BFGS method is based on the BFGS method which stores and transports the inverse Hessian approximation as a dense matrix. Specifically, the search direction in RBFGS is $\eta_k = -\mathcal{B}_k^{-1} \operatorname{grad} f(x_k)$, where $\mathcal{B}_k$ is a linear operator that approximates the action of the Hessian on $\mathrm{T}_{x_k} \mathcal{M}$. $\mathcal{B}_k$ requires a rank-two update at each iteration, see [20, Algorithm 1] for the update formula. Unlike BFGS, the limited-memory version of BFGS stores only some relatively small number of vectors that represent the approximation implicitly. Therefore LRBFGS is appropriate for large-size problems, due to its benefit in reducing storage requirements and computation time per iteration.

As a continuation of our work in [38], we provide specific LRBFGS for the SPD Karcher mean

Algorithm 4 RBB for the SPD Karcher mean computation using extrinsic representation [22]

Input: backtracking reduction factor $\varrho \in (0,1)$; Armijo parameter $\delta \in (0,1)$; initial iterate $x_0 \in \mathcal{S}_{++}^{\mathrm{n}}$; the first stepsize α_0^{BB};

1: $k = 0$;
2: Compute $f(x_k)$, $\operatorname{grad} f(x_k)$;
3: **while** $\|\operatorname{grad} f(x_k)\| > \epsilon$ **do**
4: Set stepsize $\alpha_k = \alpha_k^{BB}$;
5: Set $\eta_k = -\operatorname{grad} f(x_k)$; ▷ # w
6: If $$\|\operatorname{grad}\operatorname{grad} f(x_k)\| / \|\operatorname{grad} f(x_0)\| < accuracy$$ then set $x_{k+1} = x_k \exp(\alpha_k x_k^{-1} \eta_k)$ and go to Step 10;
7: Compute $\tilde{x}_k = x_k \exp(\alpha_k x_k^{-1} \eta_k)$; ▷ # $61n^3/3$
8: If $$f(\tilde{x}_k) \leq f(x_k) + \delta \alpha_k g(\operatorname{grad} f(x_k), \eta_k),$$ then set $x_{k+1} = \tilde{x}_k$ and go to Step 10;
9: Set $\alpha_k = \varrho \alpha_k$ and go to Step 7;
10: Compute $\operatorname{grad} f(x_{k+1})$;
11: Compute $s_k = \alpha_k \eta_k \exp(\alpha_k x_k^{-1} \eta_k)$, $y_k = \operatorname{grad} f(x_{k+1}) + \eta_k \exp(\alpha_k x_k^{-1} \eta_k)$; ▷ # $2n^3 + n^2$
12: Compute $\alpha_{k+1}^{BB} = g(s_k, s_k)/g(s_k, y_k)$; ▷ # $12n^3$
13: Set $\alpha_{k+1}^{BB} = \min\{\alpha_{max}, \max\{\epsilon, \alpha_{k+1}^{BB}\}\}$ if $g(s_k, y_k) > 0$; otherwise, $\alpha_{k+1}^{BB} = \alpha_{max}$;
14: $k = k + 1$;
15: **end while**

computation in Algorithm 6 and 7, so that readers are able to implement the methods conveniently. In fact, those two algorithms are ready to solve any optimization problems on $\mathcal{S}_{++}^{\mathrm{n}}$ as long as the readers provide a cost function and its Riemannian gradient. Algorithm 6 uses the extrinsic representation, and Algorithm 7 uses the intrinsic representation. The number of flops for each step is given on the right-hand side of the algorithms. For simplicity of notation, we use λ_m, λ_r, and λ_t to denote the flops in the metric, retraction, and vector transport evaluations respectively, and use superscripts, w and d, to denote the extrinsic and intrinsic representations respectively. The numbers of flops per iteration for Algorithm 6 and Algorithm 7, respectively, are

$$\#^w = 2(l+2)\lambda_m^w + 4lw + \lambda_r^w + 4w + 2(l+1)\lambda_t^w, \tag{4.5}$$

$$\#^d = 2(l+2)\lambda_m^d + 4ld + \lambda_r^d + 4d + (13n^3/3 + 2d). \tag{4.6}$$

Notice that m is the upper limit of the limited-memory size l. Also notice that there is no λ_t^d term in equation (4.6) since the vector transport by parallelization is used, which is the identity. The last term $(13n^3/3 + 2d)$ in (4.6) comes from the evaluation of functions $E2D$ and $D2E$ given in Algorithm 1 and 2. For the metric evaluation, we have $\lambda_m^w = 6n^3 + o(n^3)$ and $\lambda_m^d = n^2 + o(n^2)$ for different representations. Simplifying and rearranging (4.5) and (4.6), we have

$$\#^w = 12ln^3 + 24n^3 + \lambda_r^w + 2(l+1)\lambda_t^w + o(ln^3) + o(n^3), \tag{4.7}$$

$$\#^d = 4ln^2 + 13n^3/3 + \lambda_r^d + o(ln^2) + o(n^3). \tag{4.8}$$

From (4.7) and (4.8), the computational benefit of the intrinsic representation is substantial. The limited-memory size l imposes a much heavier burden on Algorithm 6 where the extrinsic representation is used. In our implementation of Algorithm 7, we suggest retraction (3.4), which needs

Algorithm 5 RBB for the SPD Karcher mean computation using intrinsic representation and vector transport by parallelization

Input: backtracking reduction factor $\varrho \in (0,1)$; Armijo parameter $\delta \in (0,1)$; initial iterate $x_0 \in \mathcal{M}$; the first stepsize α_0^{BB};

1: $k = 0$;
2: Compute $\mathrm{grad}\, f(x_k)$;
3: Compute $x_k = L_k L_k^T$; ▷ $\# n^3/3$
4: Compute $\mathrm{gf}_k^d = E2D_{x_k}(\mathrm{grad}\, f(x_k))$ by Algorithm 1; ▷ $\#\ 2n^3 + d$
5: **while** $\|\mathrm{gf}_k^d\| > \epsilon$ **do**
6: Set stepsize $\alpha_k = \alpha_k^{BB}$;
7: Set $\eta_k = -\mathrm{gf}_k^d$; ▷ $\# d$
8: Compute $\eta_k^w = D2E_{x_k}(\eta_k)$ by Algorithm 2; ▷ $\# 2n^3 + n(n+1)/2$
9: If $\|\mathrm{gf}_k^d\| / \|\mathrm{gf}_0^d\| < accuracy$
then set $x_{k+1} = R_{x_k}(\alpha_k \eta_k^w)$ using (3.4) and go to Step 13;
10: Compute $\tilde{x}_k = R_{x_k}(\alpha_k \eta_k^w)$ using (3.4) ; ▷ $\#\ 3n^3 + 3n^2$
11: If $f(\tilde{x}_k) \leq f(x_k) + \delta \alpha_k \eta_k^T \mathrm{gf}_k^d$,
then set $x_{k+1} = \tilde{x}_k$ and go to Step 13;
12: Set $\alpha_k = \varrho \alpha_k$ and go to Step 10;
13: Compute $\mathrm{grad}\, f(x_{k+1})$;
14: Compute $x_{k+1} = L_{k+1} L_{k+1}^T$; ▷ $\# n^3/3$
15: Compute $\mathrm{gf}_k^d = E2D_{x_k}(\mathrm{grad}\, f(x_k))$ by Algorithm 1; ▷ $\#\ 2n^3 + d$
16: Compute $s_k = \alpha_k \eta_k$, $y_k = \mathrm{gf}_{k+1}^d - \mathrm{gf}_k^d$; ▷ $\# 2d$
17: Compute $\alpha_{k+1}^{BB} = s_k^T s_k / s_k^T y_k$; ▷ $\#\ 4d$
18: Set $\alpha_{k+1}^{BB} = \min\{\alpha_{max}, \max\{\epsilon, \alpha_{k+1}^{BB}\}\}$ if $g(s_k, y_k) > 0$; otherwise, $\alpha_{k+1}^{BB} = \alpha_{max}$;
19: $k = k + 1$;
20: **end while**

$3n^3 + o(n^3)$ flops. Hence the overall flops required by Algorithm 7 is $\#^d = 4ln^2 + 22n^3/3 + o(ln^2) + o(n^3)$. Notice that if the locking condition is imposed on Algorithm 7, extra $12(l+1)n^2$ flops are needed. For Algorithm 6, any choice of retraction and vector transport would yield a larger flop compared to Algorithm 7. Notice that the identity vector transport using extrinsic representation is not applicable since it is not isometric under metric (1.1).

However, our complexity analysis above focuses on manifold- and algorithm-related operations, the problem-related operations—function, gradient evaluations and line search procedure—are not considered. From the discussion in Section 3.3, the evaluation of the cost function requires $18Kn^3$ flops, and the computation of the gradient requires extra $5Kn^3$ flops given the function evaluation. The line search procedure may take a few steps to terminate, and each step requires one cost function evaluation. In the ideal case where the initial stepsize satisfies the Armijo condition in Step 21 in Algorithm 7, i.e., the cost function is evaluated only once, the flops required by problem-related operations is $23Kn^3$. As n gets larger, the proportion of computational time spent on function and gradient evaluations is

$$\frac{23Kn^3}{23Kn^3 + 4ln^2 + 22n^3/3} \approx \frac{23K}{23K + 22/3} \geq \frac{23 \cdot 3}{23 \cdot 3 + 22/3} \approx 90.39\%. \tag{4.9}$$

Inequality (4.9) implies that the problem-related operations dominate the computation time for matrices with high dimension, which is consistent with our empirical observations in experiments that $70\% - 90\%$ of the computational time is from function and gradient evaluations. If the line search procedure requires more steps to terminate, then the problem-related operations would result in a larger proportion of total computational time. Therefore, it is crucial to have a good initial stepsize.

Finally, note that LRBFGS with zero memory size, i.e., $m = 0$, is equivalent to RBB. This is easy to verify by setting $m = 0$ in Algorithm 6 and 7. Just as there are different versions of the BB stepsize, alternatives are available for the initial scalling γ_{k+1} in step 24 of Algorithm 6 and step 29 of Algorithm 7, such as BB1 (4.2), BB2 (4.3), and $\mathrm{ABB}_{\min}$ (4.4). In particular, we use BB2 (4.3) as the default.

5 Experiments

In this section, we compare the performance of LRBFGS described in Algorithm 7 and existing state-of-the-art methods, including the Riemannian Barzilai-Borwein method (RBB) provided in [22] (using implementation in Algorithm 5), the Riemannian steepest descent method with stepsize selection rule proposed by Q. Rentmeesters et al. (RSD-QR) in [33, Section 3.6], the Richardson-like iteration (RL) of [7], and the Riemannian BFGS method (RBFGS) presented in [18, 20].

All experiments are performed on the Florida State University HPC system using Quad-Core AMD Opteron(tm) Processor 2356 2.3GHz. Experiments in Section 5.2 are carried out using

[6] If the locking condition is imposed, then $y_k^{(k+1)} = \mathrm{grad}\, f(x_{k+1})/\beta_k - \mathcal{T}_{\alpha_k \eta_k} \mathrm{grad}\, f(x_k)$, where $\beta_k = \|\alpha_k \eta_k\| / \|\mathcal{T}_{R_{\alpha_k \eta_k}} \alpha_k \eta_k\|$.

[7] If retraction (3.4) and isometric vector transport (3.12) that satisfy the locking condition are used, s_k and y_k are computed as follows: compute $z^w = \mathcal{T}_{R_{\alpha_k \eta_k^w}} (\alpha_k \eta_k^w)$, where $\mathcal{T}_{R_\xi} \eta = \eta + (\eta X^{-1} \xi + \xi X^{-1} \eta)/2$; obtain the intrinsic representation z of z^w by Algorithm 1; compute $\beta = \alpha_k^2 \eta_k^T \eta_k / z^T z$, $v_1 = 2\alpha_k \eta_k$, $v_2 = -\alpha_k \eta_k - \beta z$; Define $s_k = (I - 2v_2 v_2^T / v_2^T v_2)(I - 2v_1 v_1^T / v_1^T v_1)(\alpha_k \eta_k)$, $y_k = \mathrm{gf}_{k+1}^d / \beta - (I - 2v_2 v_2^T / v_2^T v_2)(I - 2v_1 v_1^T / v_1^T v_1)\mathrm{gf}_k^d$.

Algorithm 6 LRBFGS for problems on $\mathcal{S}^{\mathrm{n}}_{++}$ manifold using extrinsic representation and general vector transport

Input: backtracking reduction factor $\varrho \in (0,1)$; Armijo parameter $\delta \in (0,1)$; initial iterate $x_0 \in \mathcal{M}$; an integer $m > 0$;

1: $k = 0$, $\gamma_0 = 1$, $l = 0$;
2: Compute $\operatorname{grad} f(x_k)$;
3: **while** $\|\operatorname{grad} f(x_k)\| > \epsilon$ **do**
4: $\mathcal{H}^0_k = \gamma_k \,\mathrm{id}$. Obtain $\eta_k \in \mathrm{T}_{x_k}\mathcal{M}$ by the following algorithm, Step 5 to Step 15:
5: $q \leftarrow \operatorname{grad} f(x_k)$;
6: **for** $i = k-1, k-2, \dots, k-l$ **do** $\triangleright$ # $l(\lambda^w_m + 2w)$
7: $\xi_i \leftarrow \rho_i g(s^{(k)}_i, q)$;
8: $q \leftarrow q - \xi_i y^{(k)}_i$;
9: **end for**
10: $r \leftarrow \mathcal{H}^0_k q$; $\triangleright$ # w
11: **for** $i = k-l, k-l+1, \dots, k-1$ **do** $\triangleright$ # $l(\lambda^w_m + 2w)$
12: $\omega \leftarrow \rho_i g(y^{(k)}_i, r)$;
13: $r \leftarrow r + s^{(k)}_i(\xi_i - \omega)$;
14: **end for**
15: Set $\eta_k = -r$, $\alpha_k = 1$; $\triangleright$ # w
16: If $$\|\operatorname{grad} f(x_k)\|/\|\operatorname{grad} f(x_0)\| < accuracy$$ then set $x_{k+1} = R_{x_k}(\alpha_k\eta_k)$ and go to Step 20; $\triangleright$ # λ^w_r
17: Compute $\tilde{x}_k = R_{x_k}(\alpha_k\eta_k)$; $\triangleright$ # λ^w_r
18: If $$f(\tilde{x}_k) \le f(x_k) + \delta\alpha_k g(\operatorname{grad} f(x_k), \eta_k),$$ then set $x_{k+1} = \tilde{x}_k$ and go to Step 20;
19: Set $\alpha_k = \varrho\alpha_k$ and go to Step 17;
20: Compute $\operatorname{grad} f(x_{k+1})$;
21: Define $s^{(k+1)}_k = \mathcal{T}_{\alpha_k\eta_k}\alpha_k\eta_k$ and $y^{(k+1)}_k = \operatorname{grad} f(x_{k+1}) - \mathcal{T}_{\alpha_k\eta_k}\operatorname{grad} f(x_k)$; [6] $\triangleright$ # $2\lambda^w_t + 2w$
22: Compute $a = g(y^{(k+1)}_k, s^{(k+1)}_k)$ and $b = \|s^{(k+1)}_k\|^2$; $\triangleright$ # $2\lambda^w_m$
23: **if** $\frac{a}{b} \ge 10^{-4}\|\operatorname{grad} f(x_k)\|$ **then** $\triangleright$ # λ^w_m
24: Compute $c = \|y^{(k+1)}_k\|^2$ and define $\rho_k = 1/a$ and $\gamma_{k+1} = a/c$; $\triangleright$ # λ^w_m
25: Add $s^{(k+1)}_k$, $y^{(k+1)}_k$ and ρ_k into storage and if $l \ge m$, then discard vector pair $\{s^{(k)}_{k-l}, y^{(k)}_{k-l}\}$ and scalar ρ_{k-l} from storage, else $l \leftarrow l+1$; Transport $s^{(k)}_{k-l+1}, s^{(k)}_{k-l+2}, \dots, s^{(k)}_{k-1}$ and $y^{(k)}_{k-l+1}, y^{(k)}_{k-l+2}, \dots, y^{(k)}_{k-1}$ from $\mathrm{T}_{x_k}\mathcal{M}$ to $\mathrm{T}_{x_{k+1}}\mathcal{M}$ by $\mathcal{T}$, then get $s^{(k+1)}_{k-l+1}, s^{(k+1)}_{k-l+2}, \dots, s^{(k+1)}_{k-1}$ and $y^{(k+1)}_{k-l+1}, y^{(k+1)}_{k-l+2}, \dots, y^{(k+1)}_{k-1}$; $\triangleright$ # $2(l-1)\lambda^w_t$
26: **else**
27: Set $\gamma_{k+1} \leftarrow \gamma_k$, $\{\rho_k, \dots, \rho_{k-l+1}\} \leftarrow \{\rho_{k-1}, \dots, \rho_{k-l}\}$, $\{s^{(k+1)}_k, \dots, s^{(k+1)}_{k-l+1}\} \leftarrow \{\mathcal{T}_{\alpha_k\eta_k}s^{(k)}_{k-1}, \dots, \mathcal{T}_{\alpha_k\eta_k}s^{(k)}_{k-l}\}$ and $\{y^{(k+1)}_k, \dots, y^{(k+1)}_{k-l+1}\} \leftarrow \{\mathcal{T}_{\alpha_k\eta_k}y^{(k)}_{k-1}, \dots, \mathcal{T}_{\alpha_k\eta_k}y^{(k)}_{k-l}\}$; $\triangleright$ # $2l\lambda^w_t$
28: **end if**
29: $k = k+1$;
30: **end while**

Algorithm 7 LRBFGS for problems on $\mathcal{S}^{\mathrm{n}}_{++}$ manifold using intrinsic representation and vector transport by parallelization

Input: backtracking reduction factor $\varrho \in (0,1)$; Armijo parameter $\delta \in (0,1)$; initial iterate $x_0 \in \mathcal{M}$; an integer $m > 0$;

1: $k = 0$, $\gamma_0 = 1$, $l = 0$;
2: Compute $\mathrm{grad}\, f(x_k)$;
3: Compute $x_k = L_k L_k^T$; ▷ $\#n^3/3$
4: Compute $\mathrm{gf}_k^d = E2D_{x_k}(\mathrm{grad}\, f(x_k))$ by Algorithm 1; ▷ $\#\ 2n^3 + d$
5: **while** $\|\mathrm{gf}_k^d\| > \epsilon$ **do**
6: Obtain $\eta_k \in \mathbb{R}^d$, intrinsic representation of a tangent vector $\eta^w \in \mathrm{T}_{x_k}\mathcal{M}$, by the following algorithm, Step 7 to Step 17:
7: $q \leftarrow \mathrm{gf}_k^d$;
8: **for** $i = k-1, k-2, \dots, k-l$ **do** ▷ $\#\ l(\lambda_m^d + 2d)$
9: $\xi_i \leftarrow \rho_i q^T s_i$;
10: $q \leftarrow q - \xi_i y_i$;
11: **end for**
12: $r \leftarrow \gamma_k q$; ▷ $\#\ d$
13: **for** $i = k-l, k-l+1, \dots, k-1$ **do** ▷ $\#\ l(\lambda_m^d + 2d)$
14: $\omega \leftarrow \rho_i r^T y_i$;
15: $r \leftarrow r + s_i(\xi_i - \omega)$;
16: **end for**
17: set $\eta_k = -r$, $\alpha_k = 1$; ▷ $\#\ d$
18: Compute $\eta_k^w = D2E_{x_k}(\eta_k)$ by Algorithm 2; ▷ $\#\ 2n^3 + n(n+1)/2$
19: If

$$\|\,\mathrm{grad}\,\mathrm{gf}_k^d\|/\|\mathrm{gf}_0^d\| < \mathit{accuracy},$$

then set $x_{k+1} = R_{x_k}(\alpha_k \eta_k^w)$ and go to Step 23; ▷ $\#\ \lambda_r^d$
20: Compute $\tilde{x}_k = R_{x_k}(\alpha_k \eta_k^w)$; ▷ $\#\ \lambda_r^d$
21: If

$$f(\tilde{x}_k) \le f(x_k) + \delta \alpha_k \eta_k^T \mathrm{gf}_k^d,$$

then set $x_{k+1} = \tilde{x}_k$ and go to Step 23;
22: Set $\alpha_k = \varrho \alpha_k$ and go to Step 20;
23: Compute $\mathrm{grad}\, f(x_{k+1})$;
24: Compute $x_{k+1} = L_{k+1} L_{k+1}^T$; ▷ $\#n^3/3$
25: Compute $\mathrm{gf}_k^d = E2D_{x_k}(\mathrm{grad}\, f(x_k))$ by Algorithm 1; ▷ $\#\ 2n^3 + d$
26: Define $s_k = \alpha_k \eta_k$ and $y_k = \mathrm{gf}_{k+1}^d - \mathrm{gf}_k^d$;[7] ▷ $\#\ 2d$
27: Compute $a = y_k^T s_k$ and $b = \|s_k\|_2^2$; ▷ $\#\ 2\lambda_m^d$
28: **if** $\frac{a}{b} \ge 10^{-4}\|\mathrm{gf}_k^d\|_2$ **then** ▷ $\#\ \lambda_m^d$
29: Compute $c = \|y_k^{(k+1)}\|_2^2$ and define $\rho_k = 1/a$ and $\gamma_{k+1} = a/c$; ▷ $\#\ \lambda_m^d$
30: Add s_k, y_k and ρ_k into storage and if $l \ge m$, then discard vector pair $\{s_{k-l}, y_{k-l}\}$ and scalar ρ_{k-l} from storage, else $l \leftarrow l+1$;
31: **else**
32: Set $\gamma_{k+1} \leftarrow \gamma_k$, $\{\rho_k, \dots, \rho_{k-l+1}\} \leftarrow \{\rho_{k-1}, \dots, \rho_{k-l}\}$, $\{s_k, \dots, s_{k-l+1}\} \leftarrow \{s_{k-1}, \dots, s_{k-l}\}$ and $\{y_k, \dots, y_{k-l+1}\} \leftarrow \{y_{k-1}, \dots, y_{k-l}\}$
33: **end if**
34: $k = k+1$;
35: **end while**

C++, compiled with gcc-4.7.x. Section 5.4 presents a comparison of computation time between MATLAB and C++ implementations. All MATLAB experiments are performed using MATLAB R2015b (8.6.0.267246) 64-bit (glnxa64). In particular, we use the MATLAB implementation of RL in Bini et al.'s Matrix Means Toolbox[1].

Regarding the parameter setting, we set Armijo parameter $\delta = 10^{-4}$, backtracking reduction factor $\varrho = 0.5$ for well-conditioned data sets and $\varrho = 0.25$ for ill-conditioned ones, maximum stepsize $\alpha_{max} = 100$, and minimum stepsize α_{min} is machine epsilon. We mention here that it is found from our experiments (not shown in this paper) that LRBFGS is much less sensitive to ϱ than RBB for ill-conditioned problems. LRBFGS behaves similarly well over a range of values of ϱ, but for RBB, we must set $\varrho = 0.25$ to achieve satisfactory performance. The initial stepsize in the first iteration is chosen by the strategy in [33], i.e., $\alpha_0 = 2/(1 + L)$, where L is the upper bound at the initial iterate defined in inequality (2.1). For LRBFGS, we use different memory sizes m as specified in the legends of the figures, and impose the locking condition for ill-conditioned matrices. Specifically, we impose the locking condition on LRBFGS in the bottom plots of Figure 1, 2, 3, and 4. As we have shown in Section 4, imposing the locking condition requires extra complexity. For well-conditioned data sets, the problem is easy to handle, and the locking condition is not necessary. While in the ill-conditioned case, imposing the locking condition can reduce the number of iterations. The extra time caused by the locking condition is smaller than the time saved by a reduction in the number of function and gradient evaluations. The benefit of the locking condition is also demonstrated in [18]. In order to achieve sufficient accuracy, we skip the line search procedure when the iterate is close enough to the minimizer by setting $accuracy = 10^{-5}$ in Algorithm 5 and 7. Unless otherwise specified, our choice of the initial iterate is the arithmetic-harmonic mean [24] of data matrices. We run the algorithms until they reach their highest accuracy.

For simplicity of notation, throughout this section we denote the number, dimension, and condition number of the matrices by K, n, and κ respectively. For each choice of (K, n) and the range of conditioning desired, a single experiment comprises generating 5 different sets of K random $n \times n$ matrices with appropriate condition numbers, and running all 5 algorithms on each set with identical parameters. The result of the experiment is the distance to the true Karcher mean averaged over 5 sets as a function of iteration and time. To obtain sufficiently stable timing results, an average time is taken of several runs for a total runtime of at least 1 minute.

5.1 Experiment design

The experiments are designed in the same way as our previous work [38]. For each experiment, we choose a desired (true) Karcher mean μ, and construct data matrices A_i's such that their Karcher mean is exactly μ, i.e., $\sum_{i=1}^{K} \mathrm{Exp}_\mu^{-1}(A_i) = 0$ holds. The benefits of this scheme are: (i) We can control the conditioning of μ and the A_i's, and observe the influence of the conditioning on the performance of algorithms. (ii) Since μ is known, we can monitor the distance δ between μ and the iterates produced by various algorithms, thereby removing the need to consider the effects of termination criteria.

Given a Karcher mean μ, the A_i's are constructed as follows: (i) Generate W_i in Matlab, with n being the size of matrix, f the order of magnitude of the condition number, and p an integer less than n,

```
[O, ~] = qr(randn(n));
D = diag([rand(1,p)+1, (rand(1,n-p)+1)*10^(-f)]);
```

W = O * D * O'; W = W/**norm**(W, 2).

(ii) Compute $\eta_i = \mathrm{Exp}_\mu^{-1}(W_i)$. (iii) Enforce the condition $\sum_{i=1}^K \eta_i = 0$ on η_i's. (iv) Compute $A_i = \mathrm{Exp}_\mu(\eta_i)$. For more details, see [38, Section 5.1].

5.2 Comparison of performance between different algorithms using C++

We now compare the performances of all 5 algorithms on various data sets by examining results from representative experiments for different choices of (K, n, κ).

Figure 1 displays the performance results of different algorithms running on small-size problems, taking $K = 3$ and $n = 3$. Both well-conditioned ($1 \leq \kappa(A_i) \leq 20$) and ill-conditioned ($10^5 \leq \kappa(A_i) \leq 10^{10}$) data sets are tested. In the well-conditioned case, it is seen that all 5 algorithms are comparable in terms of time efficiency even though they require different numbers of iterations. For ill-conditioned matrices, RL and RSD-QR require significantly more iterations, but they are still efficient in terms of timing due to the low computational cost per iteration. RBB and LRBFGS require similar numbers of iterations, but LRBFGS with $m > 0$ takes more time. The computational complexity per iteration for Algorithm 7 with the locking condition is $23Kn^3 + 22n^3/3 + 16ln^2 + o(ln^2) + o(n^3)$ as discussed in Section 4. So when the size of the problem is small, the impact of memory size l is visible. But this is not the case when the size of the problem gets larger, as shown in Figure 2 and 3.

Figure 2 and Figure 3 report the results of tests conducted on data sets with large K ($K = 100,\ n = 3$) and large n ($K = 30,\ n = 100$) respectively. Note that when $n = 100$, the dimension of $\mathcal{S}_{++}^n$ is $d = n(n + 1)/2 = 5050$. In each case, both well- and ill-conditioned data sets are tested. For well-conditioned matrices, we observe that LRBFGS and RBB perform similarly, with a slight advantage for LRBFGS. The advantage of LRBFGS becomes larger as the matrices become increasingly ill-conditioned. Note that RBFGS is very inefficient for large n as expected and shown in Figure 3.

As the last test in this section, we compare the performances of the algorithms using two different initial iterates: the arithmetic-harmonic mean and the Cheap mean [8]. The Cheap mean is known to be a good approximation of the Karcher mean, but, is not cheap to compute. We use Bini et al.'s Matrix Means Toolbox[1] for the computation of the Cheap mean. We consider 30 badly conditioned 30×30 matrices ($10^6 \leq \kappa(A_i) \leq 10^9$). The results are presented in Figure 4. Notice that the time required to compute the initial iterate is included in the plots. The x-axis of the bottom-right plot does not start from 0, which shows that the computation of the Cheap mean is time demanding. We observe that the choice of initial iterate is crucial to RBFGS, and it affects the other algorithms in the early steps. When the initial iterate is close enough to the true solution, as shown in the bottom right plot in Figure 4, we observe a faster convergence in the first a few steps for all algorithms. In both cases, LRBFGS outperforms the other algorithms in terms of computation time and number of iterations per unit of accuracy required.

5.3 Comparison of the Riemannian metric and Euclidean metric

In this section we compare two different metrics, the Euclidean metric and Riemannian metric, for RSD, LRBFGS and RBFGS. RSD refers to the standard steepest descent in [25], and the initial stepsize is taken as the classical strategy in [37, (3.44)]. Notice that LRBFGS with $m = 0$ is RBB, i.e., RSD with the BB stepsize. Figure 5 shows the results from representative experiments for various choices of (K, n, κ). For each data set $\{A_1, \dots, A_K\}$, the majority ($> 60\%$) of the data

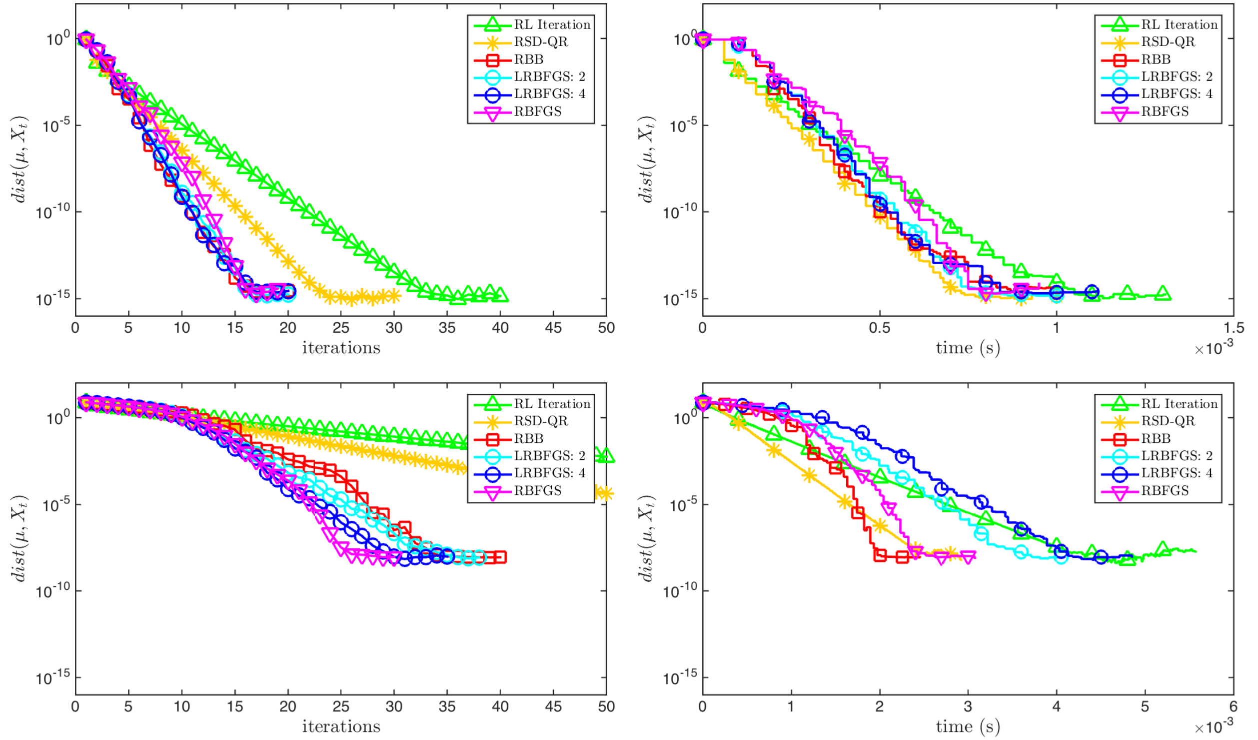

Figure 1: Evolution of averaged distance between current iterate and the exact Karcher mean with respect to time and iterations with $K = 3$, $n = 3$. Top: $1 \leq \kappa(A_i) \leq 20$; Bottom: $10^5 \leq \kappa(A_i) \leq 10^{10}$.

matrices are well-conditioned, i.e, $\kappa(A_i) < 100$. The condition number of the true Karcher mean of each set of matrices, i.e., $\mu(A_1, \ldots, A_K)$, is between 10 and 20. In the legends, 'Euc' refers to the Euclidean metric and 'Rie' refers to the Riemannian metric. We observe that the Riemannian metric shows more than 200 times faster convergence speed for RSD. When the Riemannian metric is used, LRBFGS with $m = 0$ and $m = 2$ behave similarly just as the well-conditioned case in Section 5.2. However, in the case of the Euclidean metric, LRBFGS with $m = 2$ is much faster than $m = 0$. For RBFGS, the influence of the metric becomes less significant compared to simpler methods.

5.4 Comparison of C++ and MATLAB implementations

Finally, we compare the time efficiency of the algorithms implemented by C++ and MATLAB for the SPD Karcher mean computation. The results are reported in Figure 6. The first column indicates that the C++ and MATLAB implementations are identical in terms of iterations. The second column displays the log-log plots of computation time vs. average distance between each iterate and the exact Karcher mean. For small-size problems, the C++ implementation is faster than that of MATLAB by a factor of 100 or more with the factor gradually reducing as n or K gets larger. This phenomenon can be explained by the fact that when n or K is small, the difference of efficiency between C++ and MATLAB implementations is mainly due to the difference between compiled languages and interpreted languages. When n or K gets larger, the BLAS and LAPACK

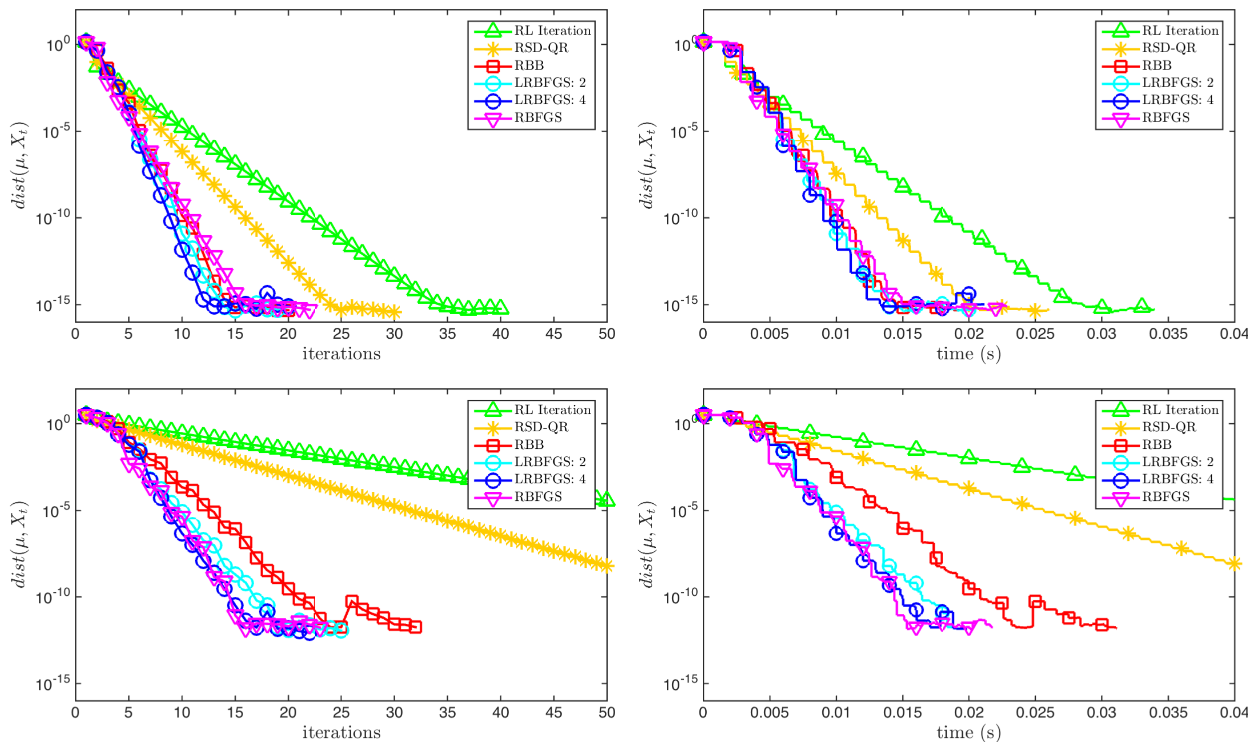

Figure 2: Evolution of averaged distance between current iterate and the exact Karcher mean with respect to time and iterations with $K = 100$ and $n = 3$; Top: $1 \leq \kappa(A_i) \leq 200$; Bottom: $10^3 \leq \kappa(A_i) \leq 10^7$.

calls start to dominate the computation time, which leads to a decrease in the factor. Note that we implement LRBFGS and RBB as a user-friendly library. It is observed that the overhead of MATLAB library machinery dominates the computation time for $k = 3$ and $n = 3$, but it becomes negligible for large-size problems.

6 Conclusion

In this paper, we consider computing the Karcher mean of SPD matrices using efficient forms of the Riemannian optimization methods. There are several alternatives from which to choose the representation of a tangent vector, retraction and vector transport. We provide complexity-based recommendations for those alternatives.

Our numerical experiments provide empirical guidelines to choose between various methods and two metrics. It is observed that RSD-QR and RL perform very well when n and K are small, and RSD-QR systematically outperforms RL. As n or K gets larger, RSD-QR and RL become less appealing, while RBB and LRBFGS single out. We recommend using LRBFGS as the default method for the SPD Karcher mean computation mainly for three reasons: (i) When the data matrices are well-conditioned, LRBFGS and RBB are competitive, with a slight advantage for LRBFGS on some test sets. (ii) As the data matrices get ill-conditioned, LRBFGS outperfroms RBB. (iii) The performance of RBB depends on the choice of parameters, such as the reduction factor ϱ in

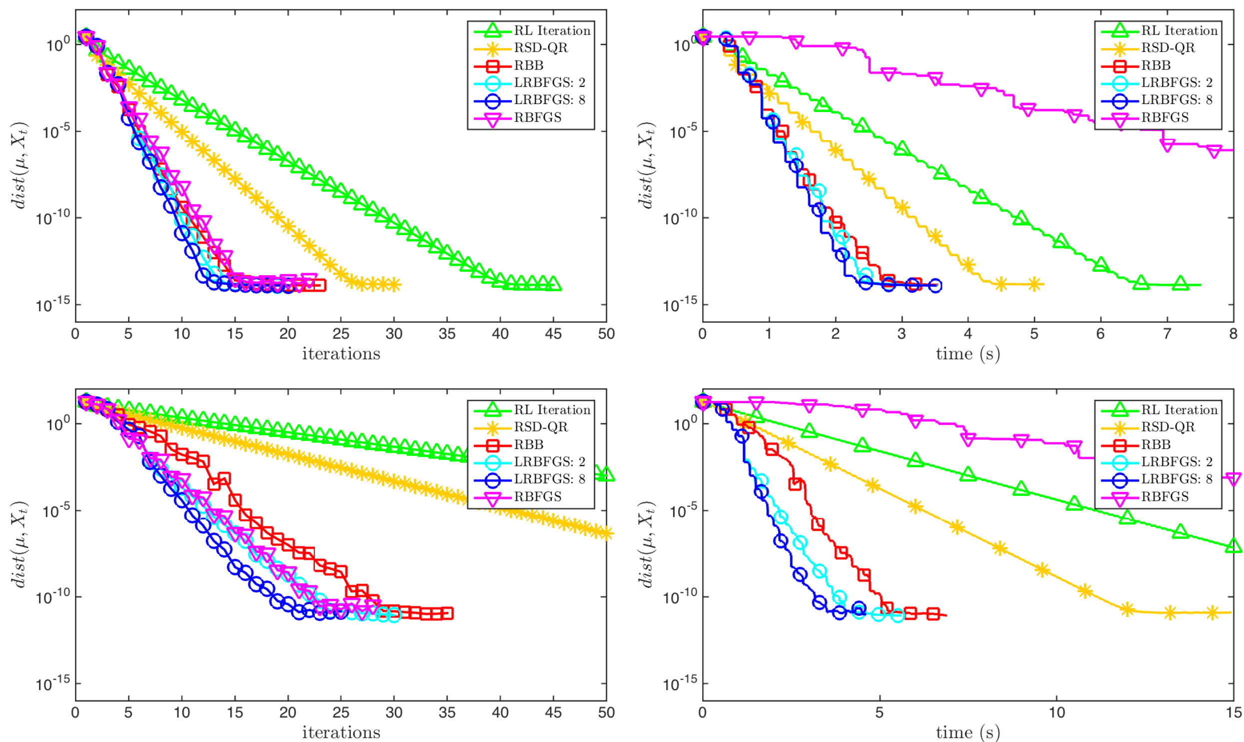

Figure 3: Evolution of averaged distance between current iterate and the exact Karcher mean with respect to time and iterations with $K = 30$ and $n = 100$; Top: $1 \leq \kappa(A_i) \leq 20$; Bottom: $10^4 \leq \kappa(A_i) \leq 10^7$.

the back tracking line search procedure, while LRBFGS is much less sensitive to parameter choices. Since RBB is in fact LRBFGS with $m = 0$, that is to say, LRBFGS can benefit from choosing $m > 0$.

We also present empirical illustration of the speedup of C++ implementation compared with MATLAB implementation. Notice that it is demonstrated theoretically and empirically that for large-size problems, the dominant computation time (70% - 90%) is in the problem-related operations, i.e., function and gradient evaluations, and therefore we conclude that our implementations of manifold- and algorithm-related objects have reached the limit of efficiency.

References

[1] P.-A. Absil and P.-Y. Gousenbourger. Differentiable piecewise-Bezier surfaces on Riemannian manifolds. Technical report, ICTEAM Institute, Universite Catholiqué de Louvain, Louvain-La-Neuve, Belgium, 2015.

[2] P.-A. Absil, R. Mahony, and R. Sepulchre. *Optimization algorithms on matrix manifolds.* Princeton University Press, 2008.

[3] T. Ando and R. Li, C.-K.and Mathias. Geometric means. *Linear Algebra and its Applications*, 385:305–334, 2004.

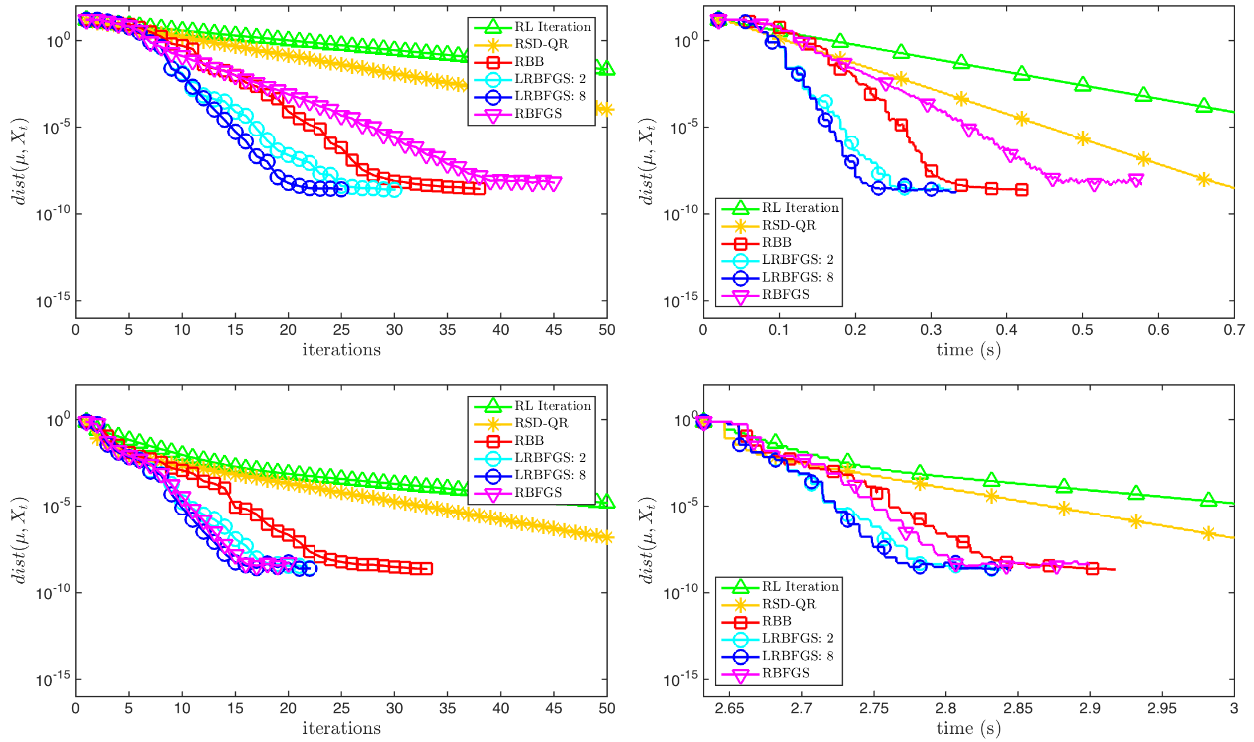

Figure 4: Comparison of different algorithms using different initial iterates with $K = 30$, $n = 30$, and $10^6 \le \kappa(A_i) \le 10^9$. Top: using the Arithmetic-Harmonic mean as initial iterate; Bottom: using the Cheap mean as initial iterate.

[4] Ognjen Arandjelovic, Gregory Shakhnarovich, John Fisher, Roberto Cipolla, and Trevor Darrell. Face recognition with image sets using manifold density divergence. In *Computer Vision and Pattern Recognition, 2005. CVPR 2005. IEEE Computer Society Conference on*, volume 1, pages 581–588. IEEE, 2005.

[5] Angelos Barmpoutis, Baba C Vemuri, Timothy M Shepherd, and John R Forder. Tensor splines for interpolation and approximation of DT-MRI with applications to segmentation of isolated rat hippocampi. *IEEE transactions on medical imaging*, 26(11):1537–1546, 2007.

[6] Rajendra Bhatia and Rajeeva L Karandikar. Monotonicity of the matrix geometric mean. *Mathematische Annalen*, 353(4):1453–1467, 2012.

[7] D. A. Bini and B. Iannazzo. Computing the Karcher mean of symmetric positive definite matrices. *Linear Algebra and its Applications*, 438(4):1700–1710, 2013.

[8] Dario Andrea Bini and Bruno Iannazzo. A note on computing matrix geometric means. *Advances in Computational Mathematics*, 35(2-4):175–192, 2011.

[9] Guang Cheng, Hesamoddin Salehian, and Baba Vemuri. Efficient recursive algorithms for computing the mean diffusion tensor and applications to DTI segmentation. *Computer Vision–ECCV 2012*, pages 390–401, 2012.

[10] Daniela di Serafinoa, Valeria Ruggierob, Gerardo Toraldoc, and Luca Zannid. On the steplength selection in gradient methods for unconstrained optimization. 2017.

[11] P. T. Fletcher and S. Joshi. Riemannian geometry for the statistical analysis of diffusion tensor data. *Signal Processing*, 87(2):250–262, 2007.

[12] P. T. Fletcher, C. Lu, S. M. Pizer, and S. Joshi. Principal geodesic analysis on symmetric spaces: statistics of diffusion tensors. *Computer Vision and Mathematical Methods in Medical and Biomedical Image Analysis*, 3117:87–98, 2004.

[13] Giacomo Frassoldati, Luca Zanni, and Gaetano Zanghirati. New adaptive stepsize selections in gradient methods. *Journal of industrial and management optimization*, 4(2):299, 2008.

[14] Gene H Golub and Charles F Van Loan. *Matrix computations*, volume 3. JHU Press, 2012.

[15] Nicholas J Higham. *Functions of matrices: theory and computation.* SIAM, 2008.

[16] Wen Huang, P-A Absil, and Kyle A Gallivan. A Riemannian symmetric rank-one trust-region method. *Mathematical Programming*, 150(2):179–216, 2015.

[17] Wen Huang, P-A Absil, and Kyle A Gallivan. Intrinsic representation of tangent vectors and vector transports on matrix manifolds. *Numerische Mathematik*, pages 1–21, 2016.

[18] Wen Huang, P-A Absil, and Kyle A Gallivan. A Riemannian BFGS method for nonconvex optimization problems. In *Numerical Mathematics and Advanced Applications ENUMATH 2015*, pages 627–634. Springer, 2016.

[19] Wen Huang, PA Absil, KA Gallivan, and Paul Hand. ROPTLIB: an object-oriented C++ library for optimization on Riemannian manifolds. Technical report, Technical Report FSU16-14, Florida State University, 2016.

[20] Wen Huang, Kyle A Gallivan, and P-A Absil. A Broyden class of quasi-Newton methods for Riemannian optimization. *SIAM Journal on Optimization*, 25(3):1660–1685, 2015.

[21] Zhiwu Huang, Ruiping Wang, Shiguang Shan, and Xilin Chen. Face recognition on large-scale video in the wild with hybrid Euclidean-and-Riemannian metric learning. *Pattern Recognition*, 48(10):3113–3124, 2015.

[22] Bruno Iannazzo and Margherita Porcelli. The Riemannian Barzilai-Borwein method with nonmonotone line-search and the Karcher mean computation. *Optimization online, December*, 2015.

[23] Sadeep Jayasumana, Richard Hartley, Mathieu Salzmann, Hongdong Li, and Mehrtash Harandi. Kernel methods on the Riemannian manifold of symmetric positive definite matrices. In *Proceedings of the IEEE Conference on Computer Vision and Pattern Recognition*, pages 73–80, 2013.

[24] B. Jeuris and R. Vandebril. Geometric mean algorithms based on harmonic and arithmetic iterations. In F. Nielsen and F. Barbaresco, editors, *Geometric Science of Information: First International Conference, GSI 2013, Paris, France, August 28-30, 2013. Proceedings*, pages 785–793. Springer Berlin Heidelberg, Berlin, Heidelberg, 2013.

[25] B. Jeuris, R. Vandebril, and B. Vandereycken. A survey and comparison of contemporary algorithms for computing the matrix geometric mean. *Electronic Transactions on Numerical Analysis*, 39:379–402, 2012.

[26] H. Karcher. Riemannian center of mass and mollifier smoothing. *Communications on Pure and Applied Mathematics*, 1977.

[27] J. Lawson and Y. Lim. Monotonic properties of the least squares mean. *Mathematische Annalen*, 351(2):267–279, 2011.

[28] Jiwen Lu, Gang Wang, and Pierre Moulin. Image set classification using holistic multiple order statistics features and localized multi-kernel metric learning. In *Proceedings of the IEEE International Conference on Computer Vision*, pages 329–336, 2013.

[29] M. Moakher. On the averaging of symmetric positive-definite tensors. *Journal of Elasticity*, 82(3):273–296, 2006.

[30] Yu Nesterov. Introductory lectures on convex programming volume I: basic course. *Lecture notes*, 1998.

[31] X. Pennec, P. Fillard, and N. Ayache. A Riemannian framework for tensor computing. *International Journal of Computer Vision*, 66(1):41–66, 2006.

[32] Y. Rathi, A. Tannenbaum, and O. Michailovich. Segmenting images on the tensor manifold. In *IEEE Conference on Computer Vision and Pattern Recognition*, pages 1–8, 2007.

[33] Q. Rentmeesters. *Algorithms for data fitting on some common homogeneous spaces*. PhD thesis, PhD thesis, Universite catholiqué de Louvain, 2013.

[34] Q. Rentmeesters and P.-A. Absil. Algorithm comparison for Karcher mean computation of rotation matrices and diffusion tensors. In *19th European Signal Processing Conference*, pages 2229–2233, Aug 2011.

[35] Gregory Shakhnarovich, John W Fisher, and Trevor Darrell. Face recognition from long-term observations. In *European Conference on Computer Vision*, pages 851–865. Springer, 2002.

[36] Oncel Tuzel, Fatih Porikli, and Peter Meer. Region covariance: A fast descriptor for detection and classification. In *European conference on computer vision*, pages 589–600. Springer, 2006.

[37] S. J. Wright and J. Nocedal. *Numerical optimization*. Springer New York, 2 edition, 2006.

[38] Xinru Yuan, Wen Huang, P-A Absil, and Kyle A Gallivan. A Riemannian limited-memory BFGS algorithm for computing the matrix geometric mean. *Procedia Computer Science*, 80:2147–2157, 2016.

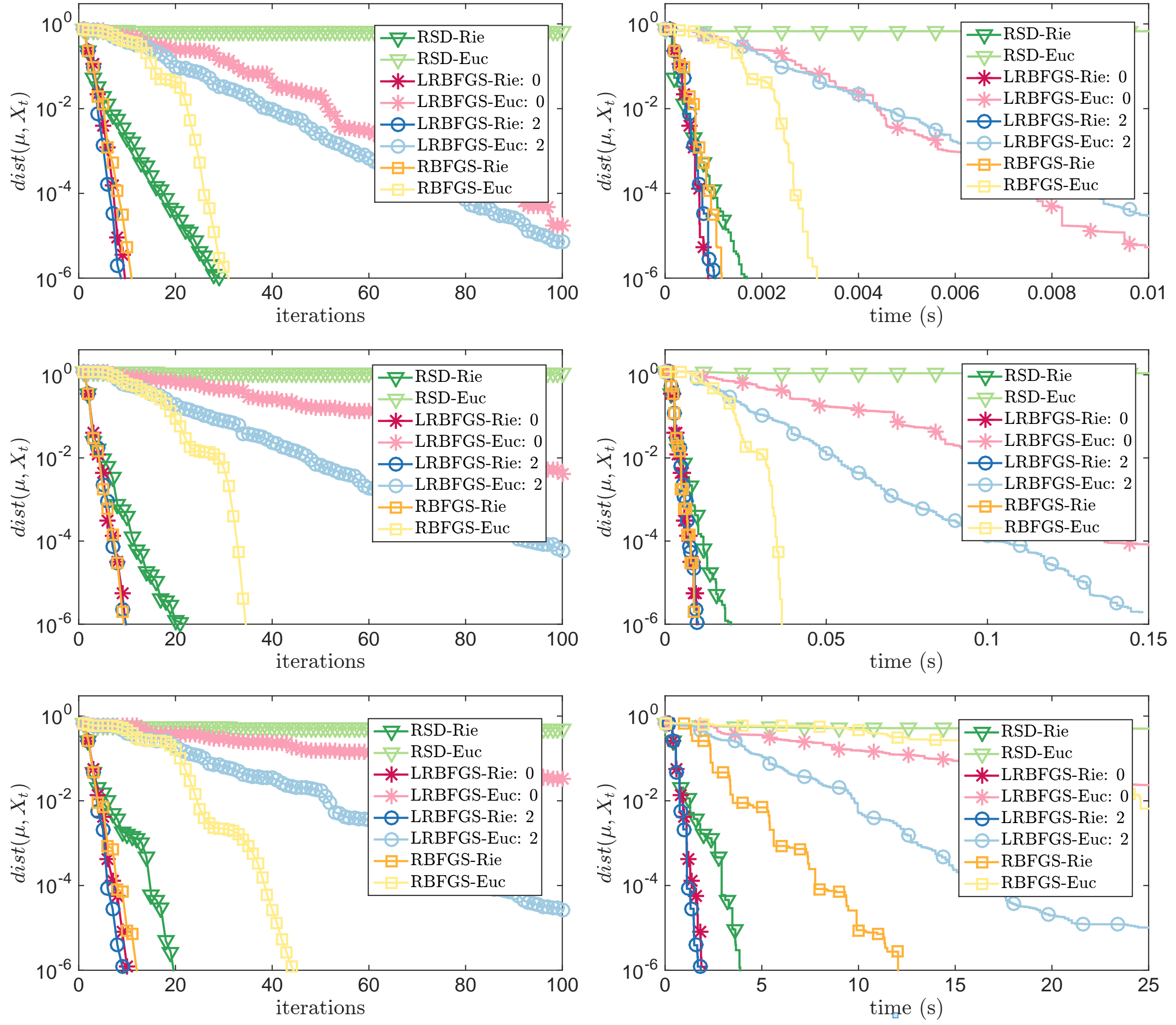

Figure 5: Comparison of different algorithms using Riemannian metric and Euclidean metric. Top row: $K = 3$, $n = 3$, and $1 \leq \kappa(A_i) \leq 10^4$; Middle row: $K = 100$, $n = 3$, and $1 \leq \kappa(A_i) \leq 10^6$; Bottom: $K = 30$, $n = 100$, and $1 \leq \kappa(A_i) \leq 10^5$.

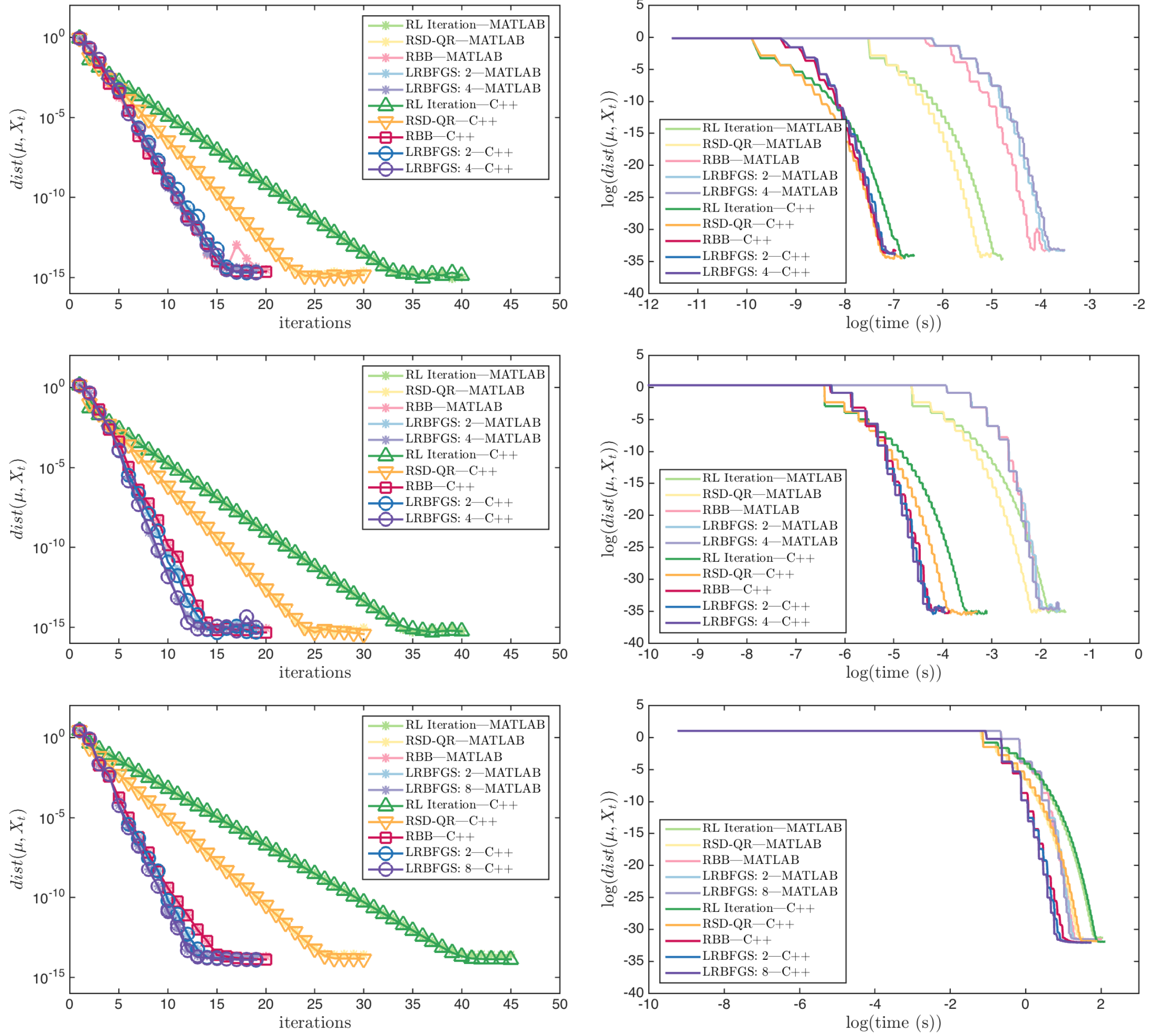

Figure 6: Comparison between C++ and MATLAB implementations with different choices of (K, n, κ). Top row: $K = 3$, $n = 3$, and $1 \le \kappa(A_i) \le 20$; Middle row: $K = 100$, $n = 3$, and $1 \le \kappa(A_i) \le 20$; Bottom: $K = 30$, $n = 100$, and $1 \le \kappa(A_i) \le 20$.